CERN 82-05
PS

CERN 82-05
Super Proton Synchrotron
Division
4 June 1982

ORGANISATION EUROPÉENNE POUR LA RECHERCHE NUCLÉAIRE
CERN EUROPEAN ORGANIZATION FOR NUCLEAR RESEARCH

RADIATION-RESISTANT MAGNETS

R.L. Keizer and M. Mottier

GENEVA
1982

© Copyright CERN, Genève, 1982

Propriété littéraire et scientifique réservée pour tous les pays du monde. Ce document ne peut être reproduit ou traduit en tout ou en partie sans l'autorisation écrite du Directeur général du CERN, titulaire du droit d'auteur. Dans les cas appropriés, et s'il s'agit d'utiliser le document à des fins non commerciales, cette autorisation sera volontiers accordée.

Le CERN ne revendique pas la propriété des inventions brevetables et dessins ou modèles susceptibles de dépôt qui pourraient être décrits dans le présent document; ceux-ci peuvent être librement utilisés par les instituts de recherche, les industriels et autres intéressés. Cependant, le CERN se réserve le droit de s'opposer à toute revendication qu'un usager pourrait faire de la propriété scientifique ou industrielle de toute invention et tout dessin ou modèle décrits dans le présent document.

Literary and scientific copyrights reserved in all countries of the world. This report, or any part of it, may not be reprinted or translated without written permission of the copyright holder, the Director-General of CERN. However, permission will be freely granted for appropriate non-commercial use.

If any patentable invention or registrable design is described in the report, CERN makes no claim to property rights in it but offers it for the free use of research institutions, manufacturers and others. CERN, however, may oppose any attempt by a user to claim any proprietary or patent rights in such inventions or designs as may be described in the present document.

ERN — Service d'information scientifique - RD/548 - 1300 - juin 1982

ABSTRACT

This is a survey of the present state of the art in the construction of radiation-resistant electromagnets, particularly for particle accelerators. A brief introduction on the electrical, mechanical, and radiochemical requirements of magnet coils is followed by the outline of a mathematical model for coil design. Details are then given of the properties of the main types of material used: inorganic cements and potting compounds, compacted metal oxides, melt spraying, high-alumina cement, asbestos cement, anodized pure aluminium. Some specific applications of the different materials are described and a detailed account is given of the techniques of magnet construction developed at CERN using concrete-impregnated asbestos.

1. INTRODUCTION

With the ever-increasing energy and intensity of accelerated beams, the problems of radiation damage and induced activity have assumed such proportions that, at critical points, magnets equipped with mineral-insulated coils have become a necessity.

Conventional coils have a radiation life of some 10^7 Gy*), which means that in severe cases of radiation damage they have to be replaced virtually every year, which is expensive in the long run. There is also the possibility that the magnet may become so radioactive that human interference, without remotely controlled equipment, is excluded.

Several laboratories have built magnets with wholly inorganic electrical insulation. They have employed simple spacer techniques, and have experimented with asbestos cement or glass-fibre-filled high-alumina cement, or have used intrinsically mineral-insulated conductors.

The technique developed at CERN is particularly suitable for long magnets, and has been applied to the construction of d.c. bending magnets and slowly pulsed quadrupoles to be used near the targets in the West and North Experimental Areas of the CERN Super Proton Synchrotron (SPS).

2. GENERAL

2.1 Technical requirements

For the realization of mineral-insulated coils, it is imperative to understand the basic principles underlying conventional coil construction. Therefore the main characteristics of the assembly and the testing of medium-tension coils, for electric potentials up to a few thousand volts between coil and ground, are described in the following sections.

Functionally, an electrical insulation may be divided into four distinct elements:

- the main dielectric, for which mica is usually employed;
- the carrier, which simplifies the wrapping of the main dielectric;
- the impregnation, which provides mechanical stability by filling all the porosities and pockets, and renders the coil impervious to moisture.

Here the tacit assumption has been made that the materials employed are non-hygroscopic. If this is not the case, the fourth element should be added, i.e.

- a leak-tight enclosure, which prevents degradation of the insulation caused by absorption of moisture.

2.1.1 Electrical requirements

The coil should withstand the inter-turn, inter-pancake, and coil-to-ground potentials during the required lifetime of the magnet. The insulation may be thin but it is still needed everywhere. During winding, very high local pressures occur at high spots, e.g. at bends and cross-over points, and the insulation is easily penetrated by small foreign particles.

The coil tests are designed to measure these characteristics. The usual tests are:

- electrical resistance check of the conductor circuit;
- induced-voltage or corona test;
- capacitor discharge test;
- insulation test between coil and ground, using a megohmmeter;
- lifetime tests by actually powering the coils for a certain time and re-measuring the characteristics.

2.1.2 Mechanical requirements

To ensure that an adequate insulation will be maintained during the lifetime, the following points have to be observed: i) the coil must be mechanically stable under magnetic and thermal forces; ii) the cooling circuit must not leak and must have an acceptable rate of corrosion; and iii) the ground-wrap must be leak-tight. Small relative movements between the conductors, due to pulsing or ripple currents, could lead to early failure.

Many coil tests have been designed for examining these mechanical properties:

- insulation-to-conductor shear tests;
- thermal cycling of the coil;
- regular sampling of brazed joints;
- choice of compatible materials from the point of view of corrosion;
- leak testing of the hydraulic circuit;
- hydraulic pulsing;
- leak testing of the ground-wrap or vacuum-tight enclosure.

There is a host of coil-mechanical questions that have never been answered adequately, on such points as:

- compatibility of the coefficients of expansion, moduli of elasticity, and the tensile strengths of the conductor and insulation;

---

*) 1 Gy (gray) = 100 rad = 1 J/kg.

- forces in the coil heads, generated by differential thermal expansion in the straight legs of the coil;
- the role of the ground-wrap in keeping the conductors together, especially near the coil heads;
- the role of shearing forces, and the fact that a mica insulation, which has no shear strength at all, still provides adequate insulation.

2.1.3 Radio-chemical requirements

In addition, for radiation-resistant coils the gases generated by radio-degradation of the constituents must diffuse out quickly enough to prevent delamination. According to Van de Voorde[1], the gas evolution in unfilled epoxy will be $2\text{–}7 \times 10^{-7}$ ml·g^{-1}·Gy^{-1}. This corresponds to 4 ml of gas per millilitre of epoxy in six hours at a dose rate of 10^{10} Gy/year. Epoxy coils are usually sufficiently porous to maintain a low pressure through diffusion of the gas, which consists mainly of H_2.

Other radiochemical problems are those of the long-term compatibility of several materials in a radiation environment, such as: fibre-glass and concrete; concrete and small amounts of humidity; or copper and magnesium oxide in close contact. Only radiation tests can provide an answer.

Still another class of problems is created when the intensity of the radiation becomes so high that ionization of the insulating medium, cooling liquid, and surrounding air occurs. In the latter case, ozone and nitrous acid are formed, and parts of the magnet which are not well ventilated will corrode. This implies that the magnet should be able to resist chemical attack by the liberated agents.

Radiolysis of the cooling water will lead to increased corrosion and deposition of the oxidation products on insulating surfaces under the influence of electric and magnetic fields.

The radiation levels and doses envisaged are of the order of 10^{10} to 10^{11} Gy received during the lifetime of the coil, which is 10 years or 50,000 hours. This is not high enough to provoke a serious change in the magnetic properties of steel or in the electrical resistance of copper, which occurs around 10^{15} to 10^{16} Gy [2].

2.2 Coil mechanics

2.2.1 Statement of the problem

Magnet coils are usually rectangular in shape and contain several windings, each conductor having a different temperature. Because the coil heads are free to move and both coil legs have the same average temperature, the stress problem reduces to that of a system of straight bars joined by a thin elastic medium.

Typically, a subsystem consists of two straight bars linked by a thin medium with longitudinal and transverse thermal gradients. The problem then would be to calculate the shearing stresses and to see what would happen if the elastic epoxy insulation would be replaced by a rigid ceramic.

This model has been investigated[3] and the results are shown in the next section.

2.2.2 Basic assumptions of the model

Consider a system of two metal bars joined by a thin elastic medium as shown in Fig. 1. The following assumptions have been made:

- The neutral plane lies in the centre of the elastic medium.
- The elastic layer is weak with respect to the metal bars and transmits shearing forces only.
- In the elastic medium the transverse thermal gradient is $\Delta T/d$, where ΔT is the temperature difference between bar 1 and bar 2.
- In the metal bars the longitudinal thermal gradient is T_g/ℓ. The system under consideration represents roughly 1/4 of the total length of one turn of a coil, hence

$$T_g = \Delta T/4 \ .$$

- For bar 1 the temperature increases by $T_1 + (x/\ell)T_g + \Delta T$ degrees, while bar 2 heats by $T_1 + (x/\ell)T_g$ degrees, where T_1 is the temperature rise of bar 2 at position $x = 0$.
- The conductor ends are free to move under the influence of forces $F_{1\ell}$ and $F_{2\ell}$.

2.2.3 Model predictions

a) *Shearing stresses.* The resulting shearing stress in the medium is then given by:

$$\tau_{\text{med}}(x) = \left(\frac{AE}{2wd} G_{\text{med}}\right)^{1/2} \left(\frac{F_{2\ell} - F_{1\ell}}{AE} + \alpha \Delta T\right) \frac{\sinh \lambda x}{\cosh \lambda \ell} \ ,$$

where A is the cross-sectional area of one bar, E is the modulus of elasticity, G_{med} the modulus of elasticity in shear, and α the coefficient of thermal expansion of the bars. The parameter λ is then defined as:

$$\lambda = \left(\frac{2wG_{\text{med}}}{dAE}\right)^{1/2} \ .$$

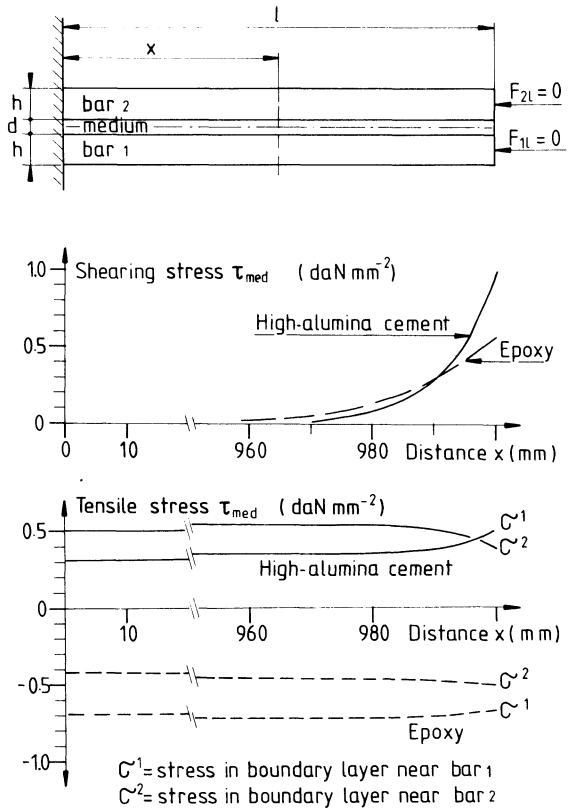

Fig. 1 Stresses in an insulating layer between two copper bars with free ends

The quantity $3/\lambda$ represents the length necessary to transfer most of the force from one bar to the next. The shearing stress is proportional to $(h/d)^{1/2}$ and, if no external forces are present, to ΔT. The maximum value appears at $x = \ell$.

Analysis of the function $\sinh \lambda x/\cosh \lambda \ell$ shows that the shearing stress is negligible all along the medium up to a distance $2/\lambda$ from the end.

If the medium fails completely at the hot end of the system, the stress peaks will move inward without diminishing appreciably in magnitude.

A distinction should be made between the maximum bonding strength of the medium to the bars and the maximum shear strength of the medium, where usually the bonding strength is the weaker of the two.

The external constraints $F_{1\ell}$ and $F_{2\ell}$ strongly influence the magnitude of τ_{med} and may even cancel the thermal effects.

With free ends, $F_{1\ell} = F_{2\ell} = 0$. The maximum peak stress is then

$$\tau_{\text{med}}(\ell) = \left(\frac{AEG_{\text{med}}}{2wd}\right)^{1/2} \alpha \Delta T \quad .$$

With the two ends linked but still free to expand, $F_{1\ell} = F_{2\ell} = whE\alpha\Delta T/2$ and $\tau_{\text{med}}(x) \equiv 0$.

For a flat coil, the conductors forming a pancake are all linked and there is no shear in the vertically oriented insulating layers. However, the conductors are not linked vertically, and if the pancakes are not cooled in parallel, shearing stresses will be created in the horizontal layers separating the pancakes.

For a saddle-shaped coil the situation is reversed—the vertical stacks of conductors are linked but not the horizontal rows.

Therefore, for both types of coils it will be necessary to have a mechanically strong ground-wrap around the coils, which increases the linkage between the conductors and thereby virtually eliminates shearing stresses.

b) *Tensile stresses.* The stresses in the outer layers of the medium that are in contact with bars 1 and 2 are given by:

$$\begin{bmatrix}\sigma^1_{\text{med}}(x)\\ \sigma^2_{\text{med}}(x)\end{bmatrix} = E_{\text{med}} \left[(\alpha - \alpha_{\text{med}}) \left(T_1 + \frac{x}{\ell} T_g + \begin{bmatrix}\Delta T\\ 0\end{bmatrix}\right)\right.$$

$$\left. \mp \alpha \frac{\Delta T}{2}\left(1 - \frac{\cosh \lambda x}{\cosh \lambda \ell}\right) - \frac{F_{1\ell}}{F_{2\ell}}\left(1 + \frac{\cosh \lambda x}{\cosh \lambda \ell}\right) - \frac{F_{2\ell}}{F_{1\ell}}\left(1 - \frac{\cosh \lambda x}{\cosh \lambda \ell}\right)\right] \quad .$$

With the ends linked, the stresses reduce to

$$\begin{bmatrix}\sigma^1_{\text{med}}(x)\\ \sigma^2_{\text{med}}(x)\end{bmatrix} = E_{\text{med}}\left[(\alpha - \alpha_{\text{med}})\left(T_1 + \frac{x}{\ell}T_g + \begin{bmatrix}\Delta T\\ 0\end{bmatrix}\right) \mp \alpha\frac{\Delta T}{2}\right] ,$$

hence a near-uniform tensile or compressive stress, depending on the sign of $(\alpha\text{-}\alpha_{\text{med}})$, all along the conductors.

With the ends free, a stress peak given by

$$\pm E_{\text{med}}\alpha\frac{\Delta T}{2}\frac{\cosh \lambda x}{\cosh \lambda \ell}$$

appears, superposed on the previous expression, at the hot end of the conductor with a maximum at $x = \ell$. At this position the total stress is given by:

$$\begin{bmatrix}\sigma^1_{\text{med}}(\ell)\\ \sigma^2_{\text{med}}(\ell)\end{bmatrix} = E_{\text{med}}(\alpha - \alpha_{\text{med}})\left(T_1 + T_g + \begin{bmatrix}\Delta T\\ 0\end{bmatrix}\right) ,$$

which is effectively the stress in an elastic layer stuck on a free hot or cold bar.

Linkage of the conductors likewise removes these stress peaks.

Examples:

In the following calculation an epoxy insulation and a high-alumina cement insulation are compared. In both cases a hollow, 8 mm bore, copper bar is used, with the following characteristics:

$w = 12.5$ mm
$h = 12.5$ mm
$A = 103$ mm^2
$d = 1$ mm
$E = 1.2 \times 10^4$ daN/mm^2
$\alpha = 16 \times 10^{-6}$/°C
$\ell = 1000$ mm.

For the cement insulation it is assumed that

$G_{\text{med}} = 800$ daN/mm^2
$E_{\text{med}} = 2000$ daN/mm^2
$\alpha_{\text{med}} = 10 \times 10^{-6}$/°C
$\bar{\sigma}_{\text{tensile}} = 1.0$ daN/mm^2
$\bar{\sigma}_{\text{compression}} = 10.0$ daN/mm^2

where $\bar{\sigma}$ represents the average breaking stress.

The epoxy insulation consists of Araldite F, HY956 hardener, and quartz-powder filler:

$G_{\text{med}} = 3/8\, E_{\text{med}}$ daN/mm^2
$E_{\text{med}} = 750$ daN/mm^2
$\alpha_{\text{med}} = 37 \times 10^{-6}$/°C
$\bar{\sigma}_{\text{tensile}} = 2.5$ daN/mm^2
$\bar{\sigma}_{\text{compression}} = 13.5$ daN/mm^2

The thermal parameters are

$$T_1 = 30\,°\text{C} , \quad \Delta T = 10\,°\text{C}.$$

The calculation yields the following transfer lengths:

epoxy: $3/\lambda = 39.9$ mm
cement: $3/\lambda = 23.6$ mm.

Figure 1 shows that the much stiffer cement yields higher shearing stresses than epoxy. The tensile stresses are equal but of opposite sign in both cases. The stress peaks at the conductor ends are less pronounced.

2.3 Materials

2.3.1 General

The four classes of materials which might be selected for electrical insulation of radiation-hardened magnets, listed in order of increasing radiation resistance, are:

- organic polymers
- inorganic cements or minerals
- inorganic glasses
- inorganic ceramics.

Some idea of the radiation resistance may be obtained from Fig. 2. The interpretation of the gamma dose is somewhat ambiguous, because the radiation damage depends on the nature of the radiation. Gamma radiation is largely absorbed in interactions with electrons. Neutrons tend to react with atomic nuclei. For the same energy absorption, the changes caused by fast neutron radiation are vastly different from those caused by gamma radiation. For example, the mechanical properties of MgO, Al_2O_3, and SiO_2 are unaffected by gamma and electron radiation at energies lower than 0.3 MeV.

The radiation resistance of organic materials, arbitrarily defined as the level at which the tensile strength is reduced to 50%, lies between 10^5 and 10^7 Gy. Radiation damage caused by scission of molecular chains and cross-linking between molecules has been extensively treated[4-6]. Some organic materials perform better in vacuum where a polyimide, such as Kapton, resists up to 4×10^8 Gy.

The inorganic cements must contain no organic binder or significant amounts of humidity so as to keep the outgassing rate low. The radiation resistance is less than that of crystalline materials because of the presence of hydroxide bonds.

Inorganic glasses are generally not suitable for large coil construction for two reasons. Firstly, the technique is complicated because the coating can only be applied after coil forming, and the temperatures are very high, rendering the process very expensive. Secondly, differential expansion of the coil will soon cause the insulation to deteriorate.

On the other hand, composite materials, such as mica-glass, are frequently used as spacers, standoffs, or ground insulation. Vitreous enamels are also used in particular cases where the geometry is simple.

Finally, the ceramics are very radiation-resistant but very limited in application unless they are melt-sprayed or used as compressed powder.

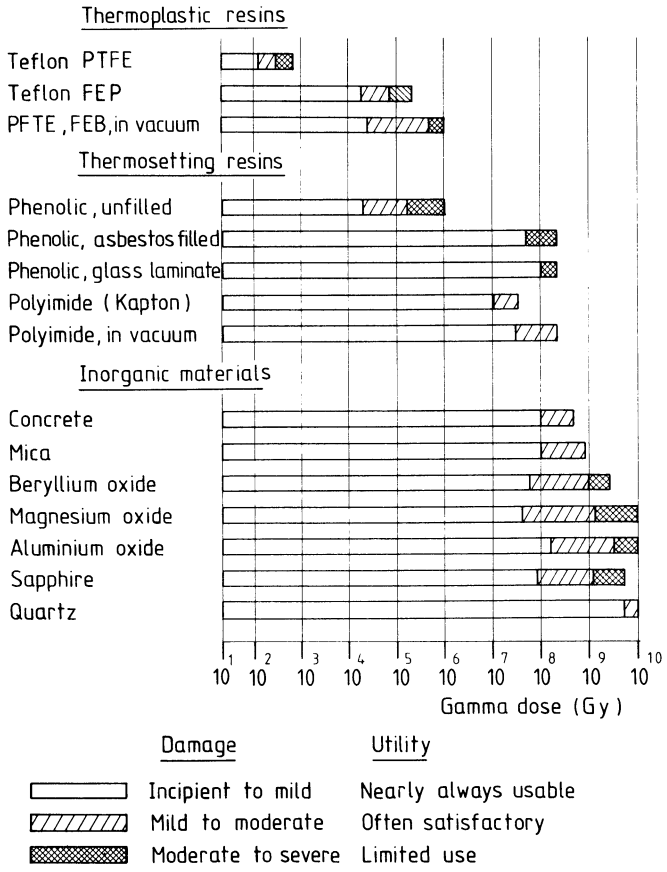

Fig. 2 Radiation resistance of several electrically insulating materials

Because of the vast choice of materials, a technical description of all commercially available cements, fibres, and sheets would occupy several volumes and therefore falls outside the scope of this report. For the most important materials, a section on technology is included which features the main characteristics and refers to existing literature. However, some materials, such as asbestos and high-alumina cement which have been used for the CERN coils, are treated in more detail.

2.3.2. Inorganic cements and potting compounds

Inorganic cements and potting compounds have been developed primarily because organic materials cannot withstand high operating temperatures.

The main characteristics of some commercially available cold-setting cements are shown in Table 1. The mechanical and dielectric strength of these compounds is generally low because of the inherent porosity, which also enhances the absorption of humidity. The relation between strength and porosity is quite general. Figure 3 shows that iron and plaster of Paris exhibit the same functional relationship. The only way to exploit the full potential of inorganic cements is to form ceramic bonds by baking at elevated temperatures and sealing the porous ceramic with an inorganic impregnation.

Table 1

Main characteristics of some cold-setting inorganic cements

Cement or potting compound	Duramic 52	Sauereisen 8	Sauereisen 29
Composition (% by weight)	Al_2O_3:95 CaO:5 SiO_2:0.1 Fe_2O_3:0.1	MgO ZrO_2 Phosphate	ZrO_2:100 Sodium-silicate:30
Composition (% of dry)	H_2O:15	H_2O:13	
Remarks	Neutral	Acid	pH 9–11
Pot life (min)	Indefinite	45–90	30–60
Shrinkage (%)	0.5	–	2–3
Porosity (% by volume)	35	–	–
Thermal expansion ($°C^{-1}$)	9×10^{-6}	2.6×10^{-6}	–
Dielectric strength (kV/mm)	2	3–4	1.2
Electric resistivity ($\Omega \cdot$ mm)	–	10^{11}–10^{12}	10^{8}–10^{9}
Tensile strength (daN/mm^2)	–	–	0.3
Compressive strength (daN/mm^2)	2.33	2.25	2.75

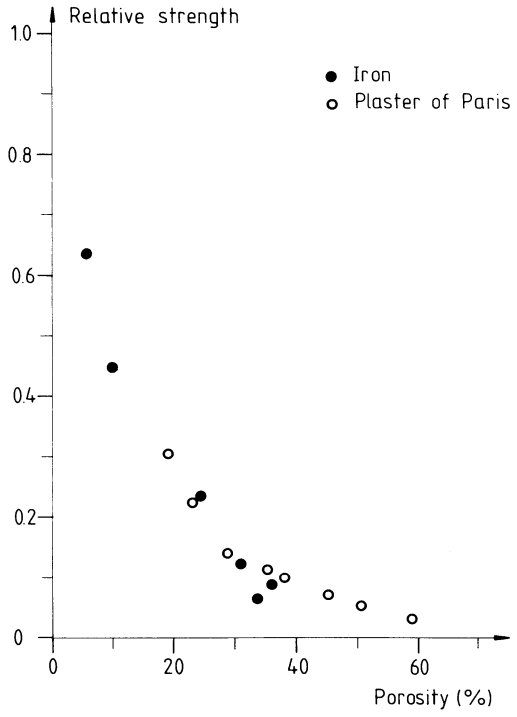

Fig. 3 The relation between porosity and relative strength of iron and plaster of Paris

Key processing factors are shrinkage upon drying and curing, pot life, and fluidity. The high shrinkage limits the application to small objects or very thin coatings. For many applications the ceramic has to be impregnated with an organic resin in order to increase the dielectric strength.

For long and voluminous objects it is much easier to use the slow-setting but strong and cheap high-alumina cement which, of course, is also porous. However, some of the more expensive cements are popular, because of the quick-setting properties, as a mounting aid or for repairing damaged coils.

Some suppliers of inorganic cements are listed in Table 2.

Table 2

Suppliers of cements and potting agents in Europe

1. Solak Chemie GmbH, Rankestrasse 26, 7000 Stuttgart 75, Fed. Rep. Germany,
   tel.: (0711) 47 23 06.
   (Represents Aremco Products, Inc., Briarcliff Manor, NY 10510, USA.)

2. Glucydor AG, 4500 Solothurn, Switzerland,
   telex: 34835; tel.: (065) 23 28 21.
   (Represents Duramic Products, Inc., Pallisades Park, NJ 07650, USA.)

3. Emerson & Cuming France, SA, 22–30 rue du Borrégo, 75015 Paris, France,
   telex: 240931; tel.: 366 59 86.

4. Kager, 6000 Frankfurt am Main 61, Fed. Rep. Germany,
   telex: 0917171; tel.: (0611) 41 41 06.

5. Schweizerische Isola-Werke, 4226 Breitenbach bei Basel, Switzerland,
   telex: 62479; tel.: (061) 80 21 81,
   and
   Isolants du Nord, 5–9 quai d'Alsace, 59506 Douai CEDEX, France,
   telex: ISONORD Douai 1171103; tel.: (27) 88 79 51.
   (Represents Sauereisen Cements Co., Pittsburgh, PA 15238, USA.)

6. Frialit-Degussit, Friedrichsfeld, Postfach 7, 6800 Mannheim 71, Fed. Rep. Germany,
   telex: 0463103; tel.: (0621) 47041.

7. EDCO, 102 place des Miroirs, 91000 Evry, France,
   telex: 600383; tel.: (60) 79 11 76.
   (Represents Adhesive Products Corp., Cleveland Ave., Albany, CA, USA.)

8. Elosol, Ltd., Dufourstrasse 101, 8034 Zurich, Switzerland,
   telex: 56245 PACOL CH; tel.: (01) 47 22 40.

9. FIRAG, Gubelstrasse 48, 8050 Zurich, Switzerland,
   telex: 56226; tel.: (01) 48 23 00.

2.3.3 Compacted metal oxides

Compacted metal oxides are used for the construction of swaged mineral-insulated cables. Table 3 lists the physical properties of a number of compressed oxides. Values for the electrical resistivity are difficult to measure at $10^{17}\ \Omega \cdot$ mm. Furthermore, small amounts of impurities strongly influence the electrical and thermal conductivity.

Of special interest is magnesia (MgO)[9-16], which is characterized by a high melting point, medium heat conductivity, high expansion, and high dielectric strength if not contaminated. The insulation contains small admixtures of boron, necessary for the manufacturing process. Magnesium oxide is used for cable construction because of its non-ageing properties.

A disadvantage is the hygroscopicity. The hydroxide $Mg(OH)_2$ is formed; this swells, and could destroy the metal sheath. The hydroxide decomposes at 350 °C. The cables therefore have to be heated to very high temperatures to restore the resistivity.

Table 3

Typical properties of compacted metal-oxide insulations

	Al_2O_3	BeO	MgO	TiO_2	ZrO_2
Melting point (°C)	2015	2530/2570	2800	1830	2600
Bulk density (g/cm³)	3.79	2.68	3.58	4.17	5.35
Heat cond. (100 °C)(W/m °C)	28.9	209	34.3	6.28	1.68
Coeff. of exp. × 10^{-6}/°C	5.5/8.0	8.0/8.4	11.0	7.5	7.2
Spec. heat ($J \cdot g^{-1} \cdot °C^{-1}$)	0.88	1.01	0.96	0.71	0.50
Dielectric strength (kV/mm)	–	–	26	–	–
Mod. of elasticity (daN/mm²)	0.010/0.036	0.031	0.008	0.008/0.010	0.025/0.017
Electric resistivity at 20 °C (Ω · mm)	10^{16}–10^{17}	–	10^{17}	–	10^{16}–10^{17}

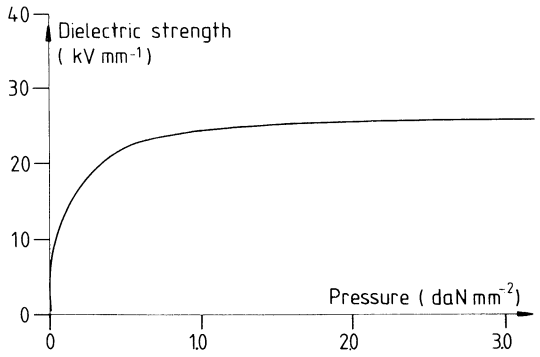

Fig. 4 The a.c. voltage strength of compressed MgO as function of the moulding pressure

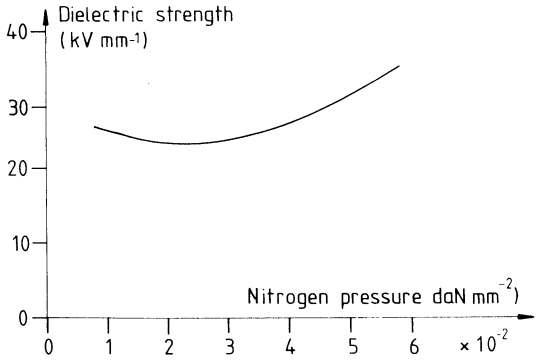

Fig. 5 The a.c. voltage strength of compressed MgO as function of nitrogen pressure

Figure 4 shows the effects of moulding pressure on a.c. voltage strength, which is determined by the presence of pores. This is also borne out by the fact that the pressure of nitrogen gas filling (see Fig. 5) strongly influences the dielectric strength.

As far as radiation is concerned, changes have been noted in the electrical resistivity, typically a tenfold decrease after a dose of 10^{12} Gy. The neutron cross-section of magnesium oxide is low.

For some applications the much harder Al_2O_3 powder is used, which tends to damage the filamentary conductors of thermocouples. Hydration does not result in volume changes.

For cable construction, magnesium silicate, BeO, ZrO_2, and ThO are also used. Zirconia has a low resistivity, and at 650 °C reacts chemically with the conductors.

Under neutron bombardment, thorium transforms into ^{233}U; it is toxic, but its resistivity is virtually temperature-independent.

2.3.4 Melt spraying[17–19]

There are several methods of spraying ceramics, grouped under the name of melt spraying. In these processes the thermal energy of a combustion reaction or an electric-arc plasma device is used to melt and project a high-velocity spray of material onto a substrate.

Several techniques have been developed:

- In flame plating, the detonation of combustible gases melts ceramic particles and propels them from a stationary gun onto a substrate. Typically, the porosity varies between 3 and 10% with a particle velocity of 800 m/s and a temperature of 3000 °C. Each detonation deposits a thickness of 5 μm.
- In torch spraying, the raw material is fed into a torch, melted, and carried to a substrate by a constant flame, yielding a porosity of 7 to 10%.
- In electric-arc plasma spraying, ceramic particles are fed into a jet by the plasma of a high-pressure d.c. arc, yielding porosities of 10 to 20% at temperatures of typically 15,000 °C.
- In induction plasma spraying, gas fed into a graphite susceptor is heated to plasma temperatures by high-frequency induction, after which the plasma itself acts as the susceptor.

An impact characteristic of the microstructure of the coatings is that the grains and pores are flattened normal to the deposition direction. The orientation results in materials with anisotropic properties which can be used to advantage. For instance, the elasticity is much higher than that of the same compound in crystalline form. This allows

the turns of helical coils to be pulled apart and to be sprayed on all sides, after which the helix is compressed to form a cylindrical coil. This cannot be done with anodized coatings.

The adherence of melt-sprayed coatings is not really understood. It is generally believed that it results primarily from the mechanical fastening of the spray particles, which is a function of the energy content. The higher the energy—thermal and kinetic—the higher will be the bond strength. The latter is dependent on the particle mass, velocity, latent heat of fusion, specific heat, and melting point of the impinging particles.

Another important parameter is the required degree of roughness and cleanliness of the receiving surface. In some cases, undercoatings of nickel-chromium or nickel-aluminium are used to provide an anchoring base. Nickel and aluminium react exothermally, thereby providing a higher particle energy level.

However, mechanical interlocking is not the only bonding mechanism. There seems to exist, in addition, an intrinsic adhesion achieved by metal-to-metal or chemical bonds. For instance, the strong adhesion of alumina and oxidized iron results from a spinel bond.

The thickness of the coating, in the case of electrical insulation, should largely exceed the surface roughness and would vary between 50 and 200 μm for plasma-sprayed alumina. For thicker coatings, the stresses caused by shrinkage of the particles after solidification will cause delamination.

Any material which does not vaporize or decompose can be melt-sprayed. For the construction of radiation-resistant magnets, not only are the non-conducting oxides—e.g. alumina, magnesia, and silica—of interest, but also some porcelain or glass compositions.

Finally, Table 4 [20] shows some physical properties of alumina, which has been used for the construction of radiation-hardened magnets at CERN. An X-ray analysis of the coating shows that no hydroxides are present. The radiation resistance should therefore be high. The base metal is not completely protected, and the coating is hygroscopic because the porosity is mainly interconnected. Ideal applications are therefore to be found in a vacuum environment. The difference between friction in air, which is high, and in vacuum, which is low, is very significant in this respect.

Table 4

Some physical parameters of melt-sprayed alumina coatings

	Torch sprayed	Plasma sprayed	Flame plated
Composition (X-ray) (%)	–	–	1–2 Al_2O_3 97 γAl_2O_3
Hardness (VPN_{300})	500	800	1100
Porosity (% by volume)	6–8	2–3	0.5–1.0
True density	3.98	3.98	3.98
Bulk density	3.24	–	3.45
Interface bond	Poor	Good	Very good
Bonding strength (daN/mm^2)	–	–	670 on Al 600 on Fe
Mod. of elasticity (daN/mm^2) (theoretical 3×10^6)	0.4×10^6	–	$0.8–1.0 \times 10^6$
Coeff. of friction in air	–	–	0.32–0.58
Coeff. of friction in vacuum	–	–	0.17–0.26
Electric resistivity ($\Omega \cdot mm$)	10^9	10^{10}	10^{14}
Dielectric strength (kV/mm)	7	13.6	15
Specific heat ($J \cdot g^{-1} \cdot ° C^{-1}$)	–	–	0.82
Coeff. of exp. (20 °C)/ $°C^{-1}$	–	–	6.55×10^{-6}
Thermal conductivity (W/m °C)	–	–	1.6–2.1

2.3.5 High-alumina cement [21]

a) *General features.* Considerable work has been carried out on the mechanical and radiation characteristics of cement or concretes[22-25]. The task of choosing between the many hydrated cements is thus simplified considerably. High-alumina cement (HAC) in conjunction with an alumina aggregate turns out to be the best choice for radiation-resistant magnets.

The chemical composition of a typical high-alumina cement is given in Table 5.

High-alumina cement has a high early strength, which renders it suitable for removal from the mould after 24 hours. Figure 6 compares the strength development of several cements, showing an order of magnitude of difference compared with Portland cement after curing for 24 hours. The rapid-hardening properties arise from the presence of calcium aluminate, with Al_2O_3CaO as the predominant compound. After hardening, there is no free hydrated lime, CaO(OH). There is a gradual loss of strength in the presence of moisture if the ambient temperature exceeds 26 °C. At high temperatures the cement loses its hydraulic bonds, which are then replaced by ceramic bonds.

Table 5

Chemical composition of high-alumina cement

Component	% by weight
Al_2O_3	43.5
Fe_2O_3, FeO, Fe_3O_4	13.1
CaO	37.5
SiO_2	3.8
MgO	0.3
Loss on ignition	0.2
Insoluble	1.2
SO_3	0.4

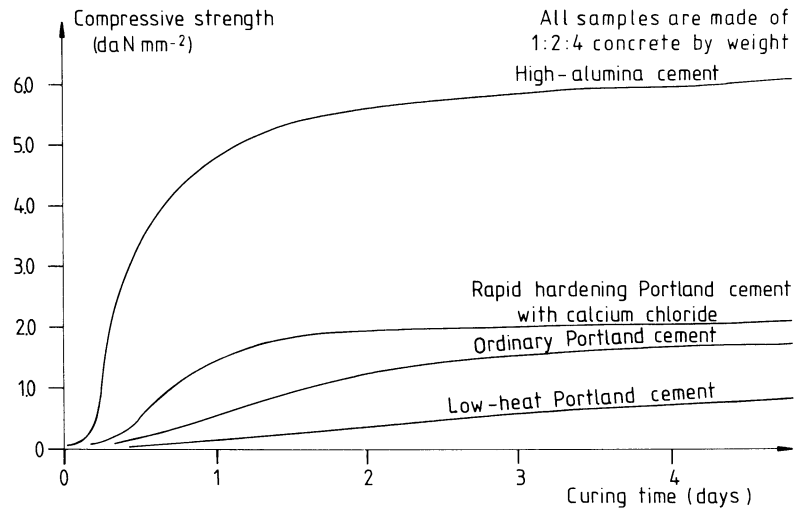

Fig. 6 The strength development of different cements

Concrete, in general, shows considerable volume change due to variation in moisture content. This can be reduced by choosing a proper aggregate and specific agents in order to suppress this effect. The concrete should be very dry for electrical applications. This invariably results in excessive cracking, especially if pure cement paste is used. Therefore concrete should never be applied in cases where tensile stresses could develop.

Radiation-resistance tests indicate that neutron doses of 10^{19} n/cm^2 (E > 1 MeV) leave samples of pure HAC[24] relatively unaffected, the main damage being caused by thermal cycling inside the reactor core rather than by neutron radiation.

The initial outgassing rate is very high for wet concrete with 5% of moisture[24]; but finally, after receiving 1.5×10^6 Gy of estimated γ-dose due to neutrons, the gas evolution drops to less than 5 ml per 10^7 Gy per kilogram of concrete. The gas mixture contains H_2 and O_2 in the volume ratio of 2:1. It is therefore important that encapsulated coils be as dry as possible.

Less important for the mechanical behaviour of the coil is the activation of cement. Tests[26] indicate that for high-energy proton facilities it is important to have a low-alkali and low-magnesium cement. The presence of flint (SiO_2) also enhances the level of induced activity.

b) *HAC grout used at CERN for coil impregnation.*The coils were impregnated in a cement bath consisting of 33% by weight of HAC mixed with water.

The coil heads were potted in a concrete made of 33% HAC, 25% natural alumina, and water. The grain size of the aggregate was 0 to 0.4 mm.

Mechanical tests were carried out on cylindrical samples of seven-day concrete. For tensile tests the length was 45 mm with a diameter of 11.5 mm, and for compression tests the respective dimensions were 20 and 19.3 mm.

The compressive strength, 13 ± 2 daN/mm^2, is high, whilst the tensile strength, 0.46 ± 0.1 daN/mm^2, is low. The latter effect is due to the high water content which is necessary for obtaining the required viscosity, and which produces a high-porosity cement. The compressive Young's modulus is 945 daN/mm^2, whilst the tensile modulus is 4000 daN/mm^2.

2.3.6 Asbestos cement

a) *Physical properties of asbestos.* Asbestos occurs naturally in many varieties, of which chrysotile, which appears in filamentary form, is of particular interest for the fabrication of flexible tape and asbestos board.

The crystal structure of chrysotile [or $(OH)_6Mg_6Si_4O_{11} \cdot H_2O$] contains water of constitution and water of hydration, and consists of alternate planes of tetrahedral silica and octahedral magnesium-hydroxide. The outer surface consists of magnesium hydroxide.

The diameter of the hollow chrysotile fibres is smaller than 2×10^{-5} mm. Therefore chrysotile provides a large surface and is a superior filler. The tensile strength is high—200 to 600 daN/mm^2. Above 400 °C the loss of crystal water, which represents 3% by weight, causes a weakening of the fibres as shown in Fig. 7. The properties of chrysotile fibres are therefore seriously impaired at temperatures exceeding 649 °C, where all the crystal water disappears. At 900 °C, after having lost its water of constitution (which represents 8% by weight), the material is converted into non-fibrous olivine with a fusion temperature of 1521 °C.

The moisture absorption in air is rapid. This is shown in Fig. 8, demonstrating the necessity for using a leak-tight envelope around an asbestos-insulated magnet coil. The reaction is reversible—heating to 100 °C during a couple of hours removes all the humidity.

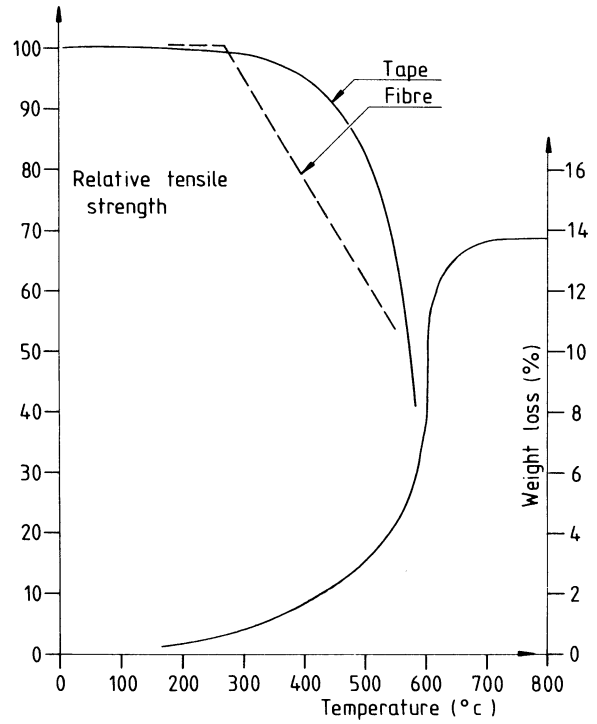

Fig. 7 The reduction of strength and weight of asbestos as function of temperature

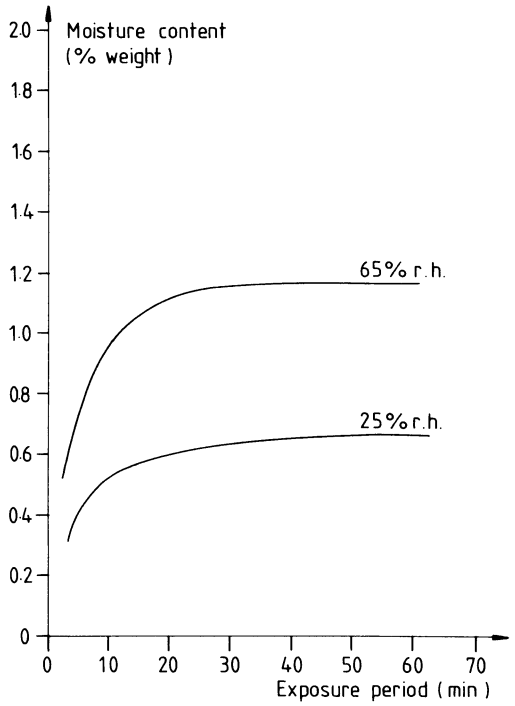

Fig. 8 Speed of moisture absorption by dry asbestos tape

No information about the radiation resistance is available. However, the presence of the hydroxide groups at positions essential to the structure of the fibres is significant. The material can therefore be classified somewhere between organic compounds and inorganic glasses, and the radiation resistance will be poor compared with that of silica or alumina.

If the asbestos tape is used as a carrier, where the loss of tensile strength is not so important, the only danger would come from excessive outgassing. Measurements on concrete, which also contains hydroxide bonds, show that the outgassing is low at the radiation levels encountered.

b) *Impregnated asbestos tape.* Tapes are available in two varieties. The most common type is reinforced with fibrous cellulosic materials and therefore cannot be used, but for special applications a 100% inorganic tape is available, which has superior thermal and chemical qualities. Both tapes, however, are treated with an organic size which should be removed. The inorganic tape sometimes also contains coloured marker threads. Heating in air to 300–350 °C for one or two hours converts most of the organic material to volatile gases; after which the tape is no longer white, but contains very little carbon.

The low tensile strength of the tape, 1.4 daN/mm^2, is only 5 to 10% of that of conventional mica-glass tape with organic binder. This imposes severe limitations on the magnitude of the forces experienced during conductor wrapping and coil forming.

The following impregnations are well known:

- Aluminium phosphate. The fibres are impregnated with high-viscosity sesqui-aluminium-phosphate $Al_{1.65}(H_{1.35}PO_4)_3$, dried and baked at 200–250 °C. The shrinkage is very high. The chemical damage to the copper and expansion due to high temperatures make this process less suitable for the construction of large coils.
- Sodium silicate. The fibres are mixed with sodium silicate, compressed, dried, and baked at 100–200 °C. The temperatures required in order to obtain a strong glassy matrix are very high. Therefore this process is also less suitable.
- Cement impregnation. For industrial applications the asbestos fibres are mixed with Portland cement or high-alumina cement grout, and then formed into sheets or tubes with oriented or random-oriented fibres. Curing may be done at room temperature and atmospheric pressure or in an autoclave.

Asbestos cement board is used for low-requirement electrical applications, such as cable ducts and arc barriers, because it is hygroscopic. If humidity is excluded it becomes a good insulation which is very strong upon compression.

For Portland-impregnated asbestos board the figures shown in Table 6 have been found in the literature.

It would be appropriate to remark that there is quite a difference between composite materials with finely divided fibres, oriented or at random, and composites where the fibres are densely packed into threads. In the latter case, much less use is made of the high tensile quality of the fibre because the cement penetrates less well between the individual fibres and does not form an interconnected matrix.

Table 6

Some physical properties of
Portland-impregnated asbestos board

Physical property	Wet	Dry
Thickness (mm)	3–25	
Specific gravity	1.55	1.95
Water absorption (% by weight)	5	17–26
Dielectric strength (kV/mm)	2	8
Modulus of elasticity (daN/mm^2)	750–1000	
Flexural strength (daN/mm^2)	1.5–4.5	
Operating temperature (°C)	300–400	
Coefficient of thermal expansion	10×10^{-6}	
Thermal conductivity (W/m °C)	0.35–0.41	
Chemical resistance to pH	> 6	

c) *Absorption tests.* After having impregnated a number of coils at CERN (see subsection 3.7.5), the following points were observed:

- The orientation of the surface to be impregnated has an influence on the insulation thickness. The vertical layers are always thinner than the horizontal layers. This so-called pile-up is caused by sedimentation of heavy cement particles on horizontal surfaces.
- In tightening up a compression mould a certain sequence is observed, whereby first the middle of the coil is compressed, and then successively the adjacent parts until the ends are reached. It would be expected that the cement is repulsed and displaced towards the end, causing an end-effect, which in fact is not observed. This shows that the trapped cement particles do not travel; only the low-viscosity water seems to travel and is released at the coil heads.
- If, instead of normal asbestos tape, the heat-treated version is used, the thickness of the insulating layer increases. This phenomenon was baptized "the tape composition effect", and is due to the stronger water-absorption of normal tape. The heat-treated tape absorbs more cement and less water, resulting in a somewhat thicker insulation.

In order to have some quantitative information, a number of experiments were carried out.

The difference in elasticity between dry and wet tapes is shown in Fig. 9. Normal tapes absorb more water than heat-treated tapes, namely 1.07 against 0.64 ml of water per gram of tape, resulting in an initial 5% difference in thickness. The figure also shows that wet tape is softer and compresses 7% more than dry tape.

The results of similar inpregnation tests on water/cement mixtures of different strengths is shown in Fig. 10. The following conclusions may be drawn:

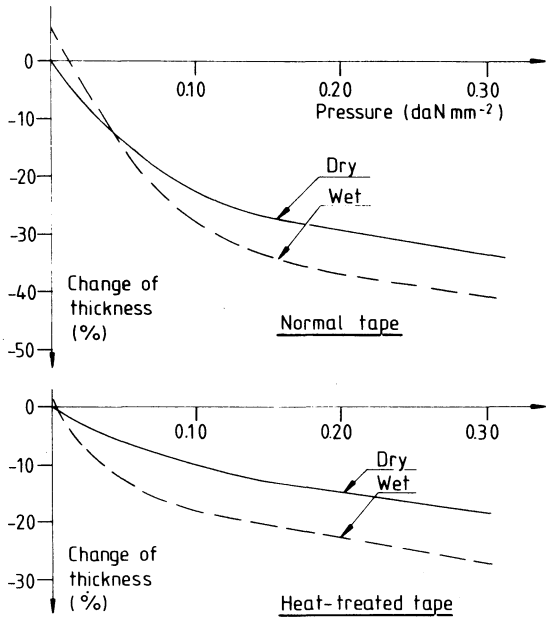

Fig. 9 Elastic behaviour of dry and wet, 0.4 mm thick, asbestos tape

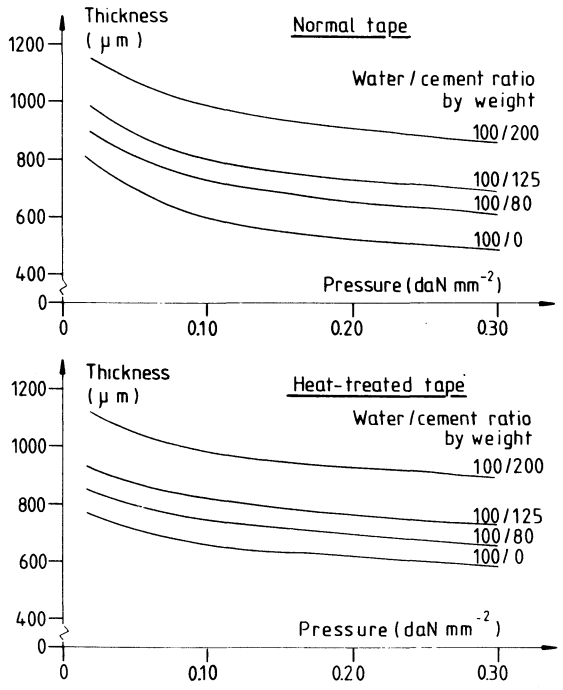

Fig. 10 Compression of two layers of impregnated, 0.4 mm thick, asbestos tape

- The thickness of the layer is proportional to the concentration of cement in the original mix, and no cement is released during compression.
- The heat-treated tape is always more rigid (this was already demonstrated in Fig. 9), and yields thicker insulating layers.
- The measured thicknesses are in good agreement with the values obtained with practical coil impregnation.
- Most of the water is released at a pressure of 0.10 daN/mm^2. The pressure mould used for the coil impregnation was therefore designed with this value in mind.

Pile-up was investigated by moving an assembly of two 16 × 16 mm conductors up and down in an agitated cement mixture during a certain time, the impregnation time, and then measuring the thickness of the compressed layer. The wrapped conductors were positioned one above the other, using 10 mm high spacers. Air bubbles coming from a system of tubes, connected to the compressed air supply and placed at the bottom of the container, kept the cement mixture in suspension (see Section 3.7.5).

The results are shown in Fig. 11. The thickness is a very sensitive function of the impregnation time.

Mixed in with pile-up is a second effect, due to a chemical reaction within the grout, which slowly increases the viscosity over a period of a few hours. The effect is demonstrated in Fig. 12. The measurements were all done with a one-minute impregnation time.

The grout therefore should be used within one hour, and the impregnation time should be limited to a few minutes in order to obtain a predetermined insulation thickness.

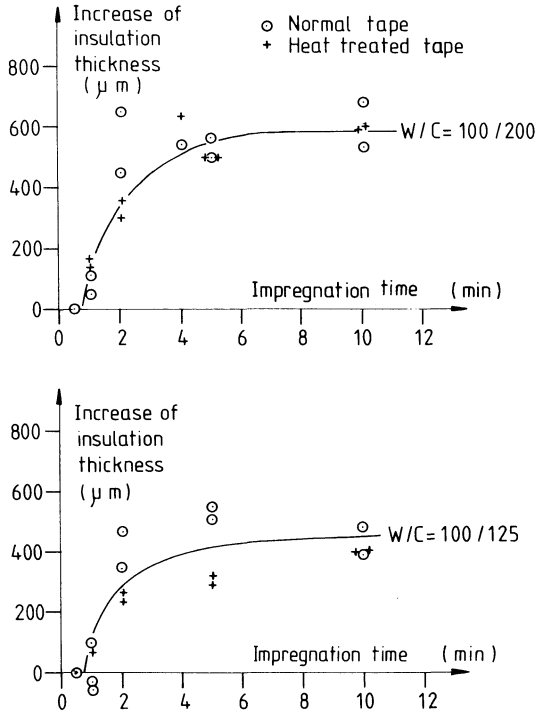

Fig. 11 Pile-up as function of the impregnation period

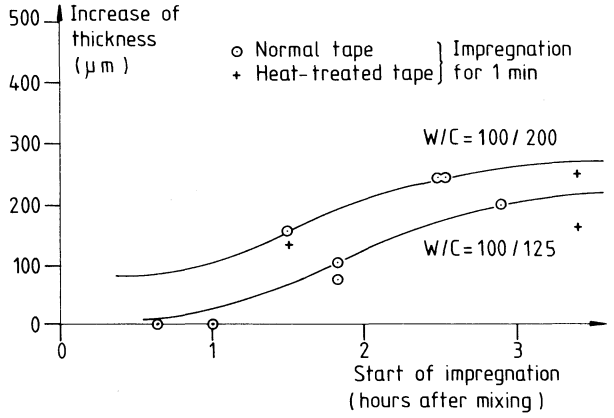

Fig. 12 Influence of initial setting on insulation thickness

2.3.7 *Anodized pure aluminium* [27-29]

The natural thickness of films of aluminium oxide on pure aluminium surfaces is 0.0025 to 0.01 μm. Anodic oxidation in a water solution containing an ionizing ionogen will increase this thickness.

If the process is carried out at low temperature, using an electrolyte which does not dissolve aluminium (borates, boric acid), a homogeneous, dense crystalline layer is formed, consisting of gamma aluminium oxides (γAl_2O_3). The thickness is a few tenths of a micron. This process is used for the formation of electrolytic capacitors.

If the oxidation is carried out using an electrolyte in which aluminium is soluble, a much thicker but porous layer is formed. This process (hard anodizing) is employed to form abrasion-resistant surfaces. The thickness ranges from 5 to 80 μm.

In industrial processes, sulfuric or oxalic acid is used as an electrolyte to form hard-anodized surfaces. The oxalic acid process is used mainly in electrical insulation applications, but sulfuric acid yields harder surfaces and has better dielectrical properties at voltages exceeding 300 V. The process of oxidation is counterbalanced by dissolution of the surface in the electrolyte. The film increases until equilibrium is reached between the two mechanisms. Figures 13 and 14 demonstrate that the lower the concentration or the temperature, the thicker will be the deposit.

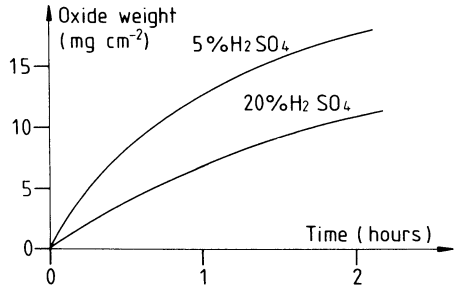

Fig. 13 The rate of film growth for anodized aluminium

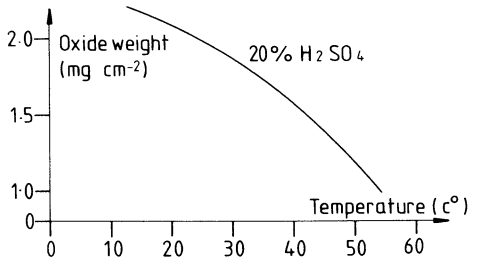

Fig. 14 The oxide film weight obtained with 240 A/m² during 15 min

The hard-anodized coating is composed of two layers:

- A thin, dense, inner layer or barrier layer consisting of gamma aluminium oxide. The thickness is 13.5 Å/V if no dissolution occurs.
- A thick, porous, outer layer of hydrated aluminium-oxide [$Al_2O_3 \cdot 3H_2O$, ($Al_2O_3 \cdot H_2O$)]. This layer is generated by the barrier layer, which is pushed outwards and swells because the volume increase is approximately 50%. On sharp edges this leads to a series of cracks and fissures, sometimes as deep as the base metal — the corner defect effect.

The temperatures are between 0 and 5 °C. Current densities of 300 to 500 A/m² are used to produce coatings of 5 to 25 μm. The electrolyte usually contains 5 to 15% sulfuric acid.

Because of the corner defect effect, the radius is limited. For a 5 μm thick coating, for instance, the minimum radius is 1.5 mm. For electrical applications, crazing is less important because the voids are filled with air.

The wear resistance is comparable to that of hardened or hard-chromed tool-steel, but it diminishes somewhat after long exposure (typically six months) to atmospheric conditions. The better the polishing, the harder and the thicker will be the oxide layer.

The heat resistance is such that the oxide can resist to short exposures of 2000 °C. In particular cases it is possible to melt the aluminium, leaving only the oxide surface.

The electrical properties, which depend very much on the surface finish, are therefore improved by polishing. Air humidity decreases the insulation resistance, but has less influence on anodized coatings than on other porous materials which do not possess a barrier layer.

The breakdown gradient is very high for thin films, where values of 800 kV/mm are reported. For hard-anodized surfaces this drops to 80–160 kV/mm. Typical breakdown voltages are 500 V for one coating of 50 μm and 700 V for two coatings, each 50 μm.

The flexibility is very poor for hard coatings but can be increased at the cost of losing abrasive resistance. Bending tests show that the deposit crazes but adheres on the tension side, but cracks and flakes on the compression side.

It is also possible to reverse the process, whereby first the surface is hard-anodized and then a gamma layer is deposited with boric acid as the electrolyte. The second layer penetrates the first one, thereby sealing the voids and pores, and a thick and dense solid dielectric is produced. Coatings of 0.5 μm thickness have been produced in this way.

Sealing is also done by boiling for 5–20 minutes in hot water in order to fill the pores with hydrated aluminium oxide. Other treatments in sodium silicate and acetic acid yield stable sealing films[30].

No information about the radiation resistance is available. It is expected that the barrier layer will stand at least 10^9 Gy, but that the porous outer layer, which contains hydroxide groups, will be reduced to amorphous alumina at lower doses.

3. TECHNIQUES

3.1 Permanent magnets

Permanent magnet quadrupole lenses are being developed for linac drift tubes[31-35]. In such cases, the performance of conventional quadrupoles is limited by the power dissipation in the coils and not by the saturation of the yoke.

The materials employed are oriented Alnico-V, barium, ferrite ceramic, platinum cobalt, and samarium cobalt. With the latter material, a gradient of 87 T/m in an aperture of 11 mm radius[32] has been obtained.

The price of these magnets varies between 1 and 10 $ per cm³, which limits its use to small-aperture magnets. The radiation resistance is high because measurable change in the magnetic properties of iron occurs only at doses of 10^{20} fast neutrons per cm² [33].

3.2 Compacted powder insulation[36-46]

Mineral-insulated cable was developed for the construction of the LAMPF accelerator beam switchyard magnets in 1972, and has since found widespread use in many other laboratories.

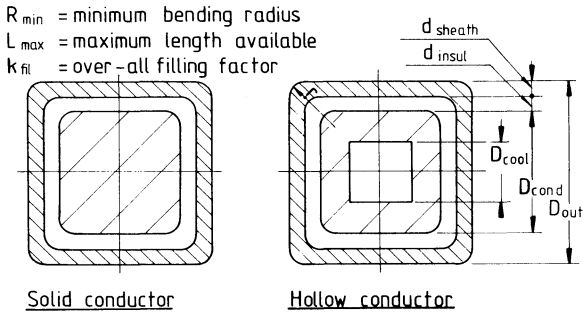

Fig. 15 Cross-section of mineral insulated cable

The construction is similar to that of the well-known immersion-heater elements or of the coaxial thermocouple wire used in the radioactive environment of nuclear reactors since many years. Instead of a circular cross-section, a square cross-section is used.

The core consists of solid or hollow oxygen-free high-conductivity copper (OFHC-Cu) surrounded by a thin layer of magnesia and a thin copper sheath, as shown in Fig. 15. Magnesia has a good radiation resistance but is hygroscopic. Sealing of the mineral-insulated cables therefore poses special problems. The final seal has to be applied immediately after drying.

Another problem is how to avoid buckling when bending the conductors. For this operation a special bending-tool should be designed, which supports the conductor on three sides.

Available conductor sizes are summed up in Table 7. There has been a steady increase in quality over the years, resulting in a thinner sheath and therefore improved heat-conducting properties of the solid cable, a better filling factor, and decreased hydraulic resistance.

The current rating for hollow conductor is not very meaningful because the ultimate value depends on the actual length of the cable and the available water pressure.

The improved current rating for solid conductor can only be obtained by potting the coil in tin solder. Special techniques are required in order to avoid hot spots.

The mineral-insulated cable has some inherent properties which render it very suitable for specific applications:

- The solid cable has a very good lateral thermal conductivity and is therefore ideally suited for indirect cooling, thus avoiding the use of ceramic feedthroughs and reducing corrosion problems.
- Operating temperatures could be very high — temperatures of 250 °C are possible.

Table 7

Some characteristics of mineral-insulated cable
Insulation resistance > 1.5 GΩ·km^{-1}
Maximum pressure = 1 daN/mm^2

D_{out} [a] (mm)	r (mm)	$D_{cond.}$ (mm)	$d_{insul.}$ (mm)	d_{sheath} (mm)	R_{min} (mm)	D_{cool} (mm)	L_{max} (m)	k_{flt} (over-all)	Specific resistance (mΩ·m^{-1})	Dielectric strength (kV_{rms})	Current (A)
6.35	1.3	3.99	0.51	0.51	12	–	305	0.326	1.31	1.25	125 [c]
6.35 [b]	0.8	4.19									330 [c]
10.48	–	6.05	1.52	0.69	25	–	198	0.282	0.556	1.50	180 [c]
10.48 [b]	–	–	–	–	–	–	–	–	–	–	500 [c]
13.45	0.8	8.89	1.52	0.76	51	–	128	0.367	0.26	1.50	300 [c]
13.45 [b]	1.6	10.67	0.76	0.51			145	0.529	0.18		545 [c]
9.52	–	5.97	1.27	0.51	32	3.30	121	0.268	0.711	1.50	400
9.52 [b]	–	–	–	–	–	–	–	–	–	–	–
13.46	1.6	9.14	1.40	0.76	32	4.57	67	0.319	0.298	1.50	750
13.46 [b]		10.03	1.02				82	0.363	0.262		1000
19.05	1.6	14.48	1.27	0.89	64	6.60	67	0.413	0.115	1.50	1800
19.05 [b]							70				

a) For the notation, see Fig. 15.
b) Improved cable with thinner sheath.
c) Current ratings obtained at SIN.

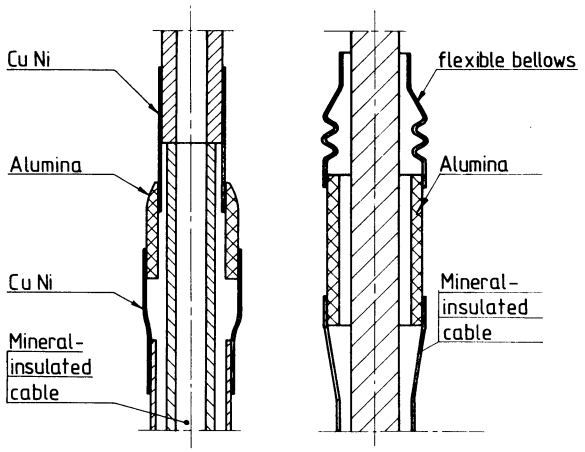

Fig. 16 Ceramic seals used for mineral-insulated cable

However, there are also some drawbacks:

- The filling factor is low, 30–40%.
- Sealing of the cable ends remains mechanically weak, but broken seals are repairable and the inherent cable insulation resistance can be restored.
- Limited lengths are available; splicing can be done only on the outside of the coils.
- The conductor dimensions are relatively inaccurate, resulting in large tolerances on water flow and resistance per unit length.
- The a.c. losses are high but can be reduced by using a stainless-steel sheath instead of a copper one.
- The breakdown voltage is rather low but suffices for most applications.

Alumina-ceramic seals developed for mineral-insulated cable are shown in Fig. 16. Adaptor pieces are necessary between the square conductor and the cylindrical ceramic, and it is possible to deform the sheath for this purpose. However, for high-temperature operation, flexible bellows seem to be more appropriate. The seals can only be mounted after coil-forming and bending of the conductor ends, because there is an appreciable axial displacement between the conductor and the sheath during bending.

3.3 Plasma-sprayed insulation

At CERN, a large number of one- to twelve-turn septum magnets have been insulated with an alumina coating, using the plasma-spray technique. The hygroscopicity of the porous coating poses no problems because the magnets are mounted in vacuum.

The cross-section of a one-turn magnet[47] is shown in Fig. 17. The core consists of three low-carbon steel blocks on which, after sandblasting, a 0.20 mm alumina coating has been deposited. Care was taken to avoid leaving sharp edges which would cause chipping. The surfaces were finished by grinding them down to 0.15 mm.

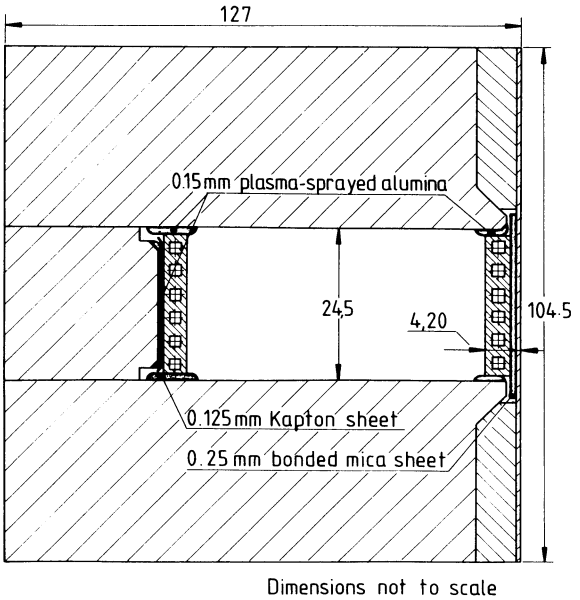

Fig. 17 Cross-section one-turn septum magnet

Impurities due to metallic particles in the alumina caused intermittent short circuits, and for this reason a 25 mm Kapton foil was inserted between the core and the return conductor.

Metallic particles come from two different sources. On the one hand, if the roughness of the sandblasted surface is of the same order as the final thickness of the alumina coating, the metal particles that remain embedded in the surface of the blocks may cause short circuits. On the other hand, metallic impurities may be released by the nozzle of the spray-gun. Therefore, before being used for insulation coating, a new nozzle should first be used for a certain length of time in order to remove loose particles. A worn nozzle also releases metal particles through fatigue.

The septum conductor is insulated by plasma-sprayed alumina on the poles, and by a bonded mica sheet inserted between the conductor and the retainer plate.

A radiation-hardened twelve-turn magnet[48] is shown in Fig. 18. Here a double electrical insulation was provided by insulating both the coil and the core. The core insulation, 0.15 mm thick, was manufactured as described above.

The coil insulation is also 0.15 mm thick, the coating being deposited on individual turns prior to assembly of the coil. The correct gap height was obtained by making the coil a few tenths of a millimetre higher than the gap, and by subsequently compressing it during assembly of the core. It turned out that the friction between the individual turns was sufficient to allow omission of the retainer plate for the septum, thereby gaining some septum thickness.

A few details might be of interest here. Examples of insulated bolts and washers, using the plasma-spray technique, are shown in Fig. 19. The 0.2 mm alumina coating is ground to size before shrinking on the outer washer. These components are much more elastic and shock-resistant than the conventional alumina washers, which require perfectly flat and parallel mating surfaces.

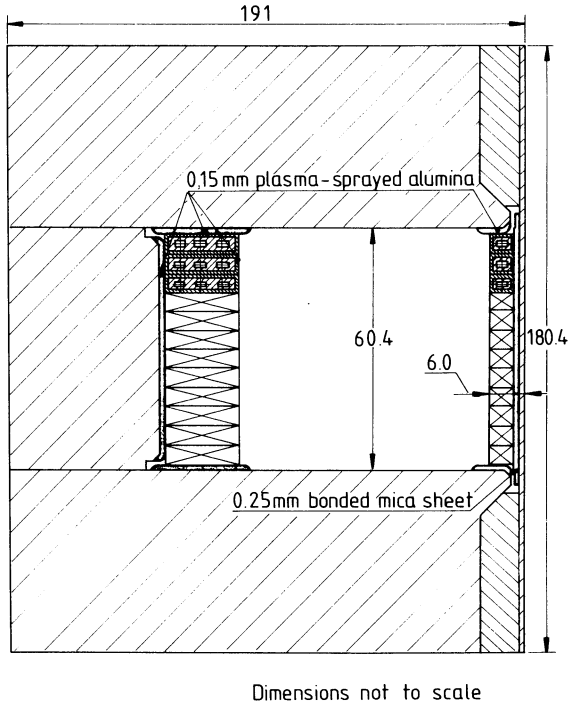

Fig. 18 Cross-section twelve-turn septum magnet

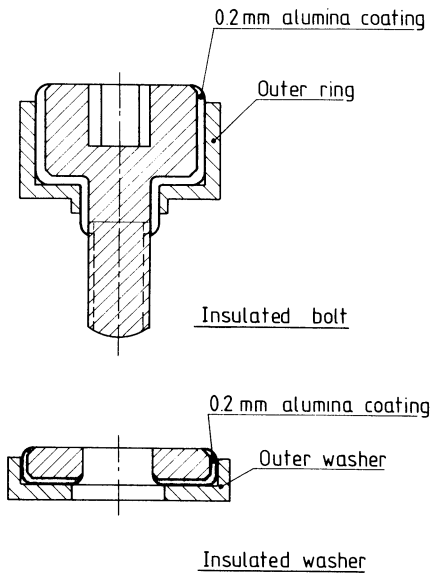

Fig. 19 Examples of insulated bolts and washers

3.4 Anodized aluminium insulation[49,50]

Anodized aluminium has found frequent application in the construction of circular lifting magnets and high-temperature excitation coils for electromagnetic devices.

Hollow aluminium conductor, hard anodized, has been used for the construction of radiation-resistant coils subjected to dose rates of 10^8–10^9 Gy/year. The ground insulation is made of anodized aluminium sheets and mica-based materials.

The advantages of using aluminium, instead of copper, are the absence of work hardening, the availability of long lengths of this material, its low residual activity, and the lower construction costs of the magnets. The disadvantages are the necessity of having either mixed cooling systems with bimetallic corrosion problems if the conductivity of the water is not sufficiently low, or having more expensive separate cooling systems. Furthermore, the conductivity of aluminium is 38–40% lower than that of copper.

The fabrication technique has to take into account the poor flexibility of anodized aluminium. The coils must be completely wound prior to anodizing. Polishing is very important, and cleaning consists of chemical etching followed by hot and cold water rinses.

The interpancake and ground insulation typically consists of 0.8 mm thick hard-anodized aluminium sheets, and strips of mica 0.5 mm thick.

Problems caused by the geometry of the bends in coil heads are prevented by using a constant radius.

Humidity was excluded by using an epoxy/fibre-glass ground-wrap in one particular construction, but could also be envisaged differently using a stainless-steel casing. For semi-porous envelopes such as fibre-glass, the cooling-water temperature should always remain above dew point.

3.5 Potted coils

Two early attempts at potting coils are known to the authors.

An ejection magnet[51], constructed for the CERN 600 MeV Synchro-cyclotron, consists of an array of 30 hollow copper tubes, diameter 30 mm, spaced more than 35 mm apart. The assembly was vibrator-cast in a C-shaped concrete block reinforced with a stainless-steel grid and aluminized stainless-steel rods.

The concrete consisted of high-alumina cement (HAC), 21.5%; alumina (Corindon), 68%; and water, 10.5%; yielding a tensile strength of 1.1 daN/mm^2 and a compressive strength of 12.0 daN/mm^2.

The aluminized copper tubes were insulated by anodizing.

The assembly was enclosed in a 3 mm thick stainless-steel box. This box was then firmly anchored in the concrete, which was dried at 80°C.

The second case is that of the Los Alamos 11-inch bending magnets[52] installed near a target receiving doses of 10^8 to 10^9 Gy/year.

The square conductors, 13 to 15 mm in cross-section, are insulated with three layers of half-lap fibre-glass tape, 0.18 mm thick. The 10 mm ground insulation is made of additional layers of fibre-glass tape and HAC.

The concrete consists of 26% HAC, 61% fused alumina, and 13% water. The vibrated coil was prestressed by heating the copper tubes to 60 °C during curing.

No cracks were observed in the outer insulation after thermal cycling and immersion tests in water.

The resistance to ground was 0.6 MΩ at 1 kV and 1 MΩ at 400 V, with the coil dry under room conditions. The resistivity of the concrete was 10^{11} Ω·mm at 80 V/mm and 0.5×10^{11} Ω·mm at 200 V/mm.

3.6 Pumped and prestressed concrete insulation

A number of short bending and quadrupole magnets[53-55] have been developed at Rutherford Laboratory or constructed for DESY, using a concrete pumping and prestressing technique for the insulation of the coils.

The concrete is pumped into an enclosed yoke structure, using the yoke and mirror plates as the pressure cylinder.

The conductor spacing is 3 mm, using mica-glass and ceramic spacers.

The high-alumina concrete, consisting of 13% HAC, 52% alumina, and 35% water, was pumped and pressurized up to 0.45 daN/mm^2. The concrete was then cured, followed by a long period of drying at temperatures exceeding 100 ° C to raise the resistivity to 10^{15} Ω·mm, after which the magnets were hermetically sealed. The dielectric strength is 7.5 kV/mm. A typical value for the insulation between windings and between coil and earth is 400 MΩ.

3.7 Cementatious impregnation

3.7.1 Introduction

The concrete flushing technique described in the last section cannot be used for long coils, because separation of the three constituents of the concrete—water, cement, and aggregate—occurs, which interrupts the flow by blocking up the ducts.

CERN therefore had to find a different way of producing long coils with cementatious insulation. The first method to be tried out was that of cement filling, in which a coil is assembled with alumina spacers and then dry cement is vibrated between the conductors by filling laterally[56]. This works well for small coils. For larger coils it is not possible to vibrate the whole coil in phase, and a homogeneous cement filling is difficult to obtain.

It was therefore decided to wrap the conductor in asbestos tape prior to winding, and to make the impregnation afterwards. This technique will be described in the following section.

Because the cementatious impregnation enters the coil from the sides, the coil has to be separated from the core. This has the advantage of reducing the risk factor, and coil repairs would be much easier should the impregnation turn out to be unsatisfactory.

Another major advantage of the technique is the possibility of replacing conventional coils in a magnet by concrete-impregnated ones without modifying the magnetic circuit.

3.7.2 Basic principles

The cross-section of a typical quadrupole coil is shown in Fig. 20. The conductor spacing is determined by a layer of 0.4 mm thick asbestos tape wrapped around each conductor. The wrapping is non-overlapping and serves only as a carrier for the impregnation.

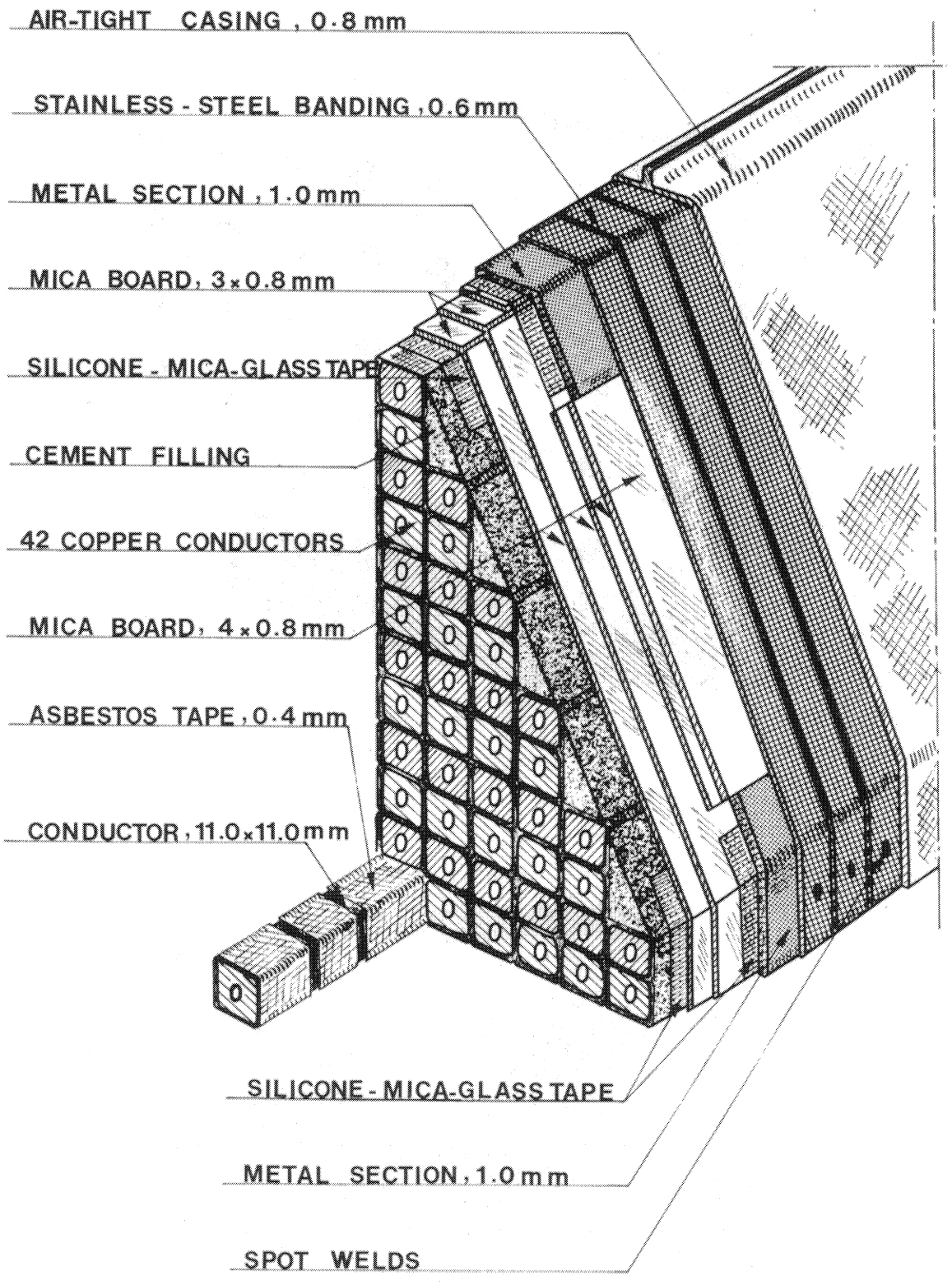

Fig. 20 QNL-B coil construction

The 0.6 to 1.0 mm wide gap is then impregnated with high-alumina cement, which adheres well to the sandblasted conductor and the asbestos tape. Other inorganic materials, such as E-glass tape, have been considered, but rejected on mechanical or chemical grounds.

The insulation is non-tracking and there is no outgassing when it is sufficiently dry, but it is rather porous. The dielectric properties of the asbestos cement may therefore be neglected, and the electrical insulation then depends on the 0.6 to 1.0 mm spacing between the conductors. This gap provides sufficient insulation, taking into account the low voltage drop between adjacent conductors, which will not exceed a few tens of volts.

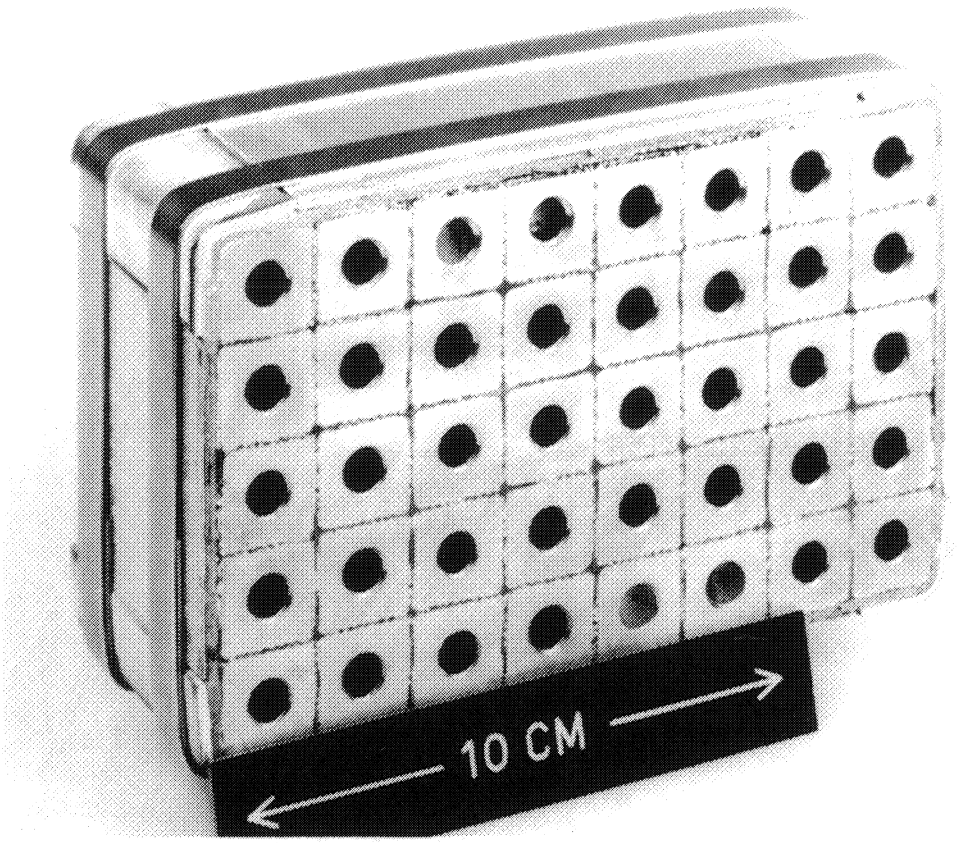

Fig. 21 The cross-section of a bending magnet coil

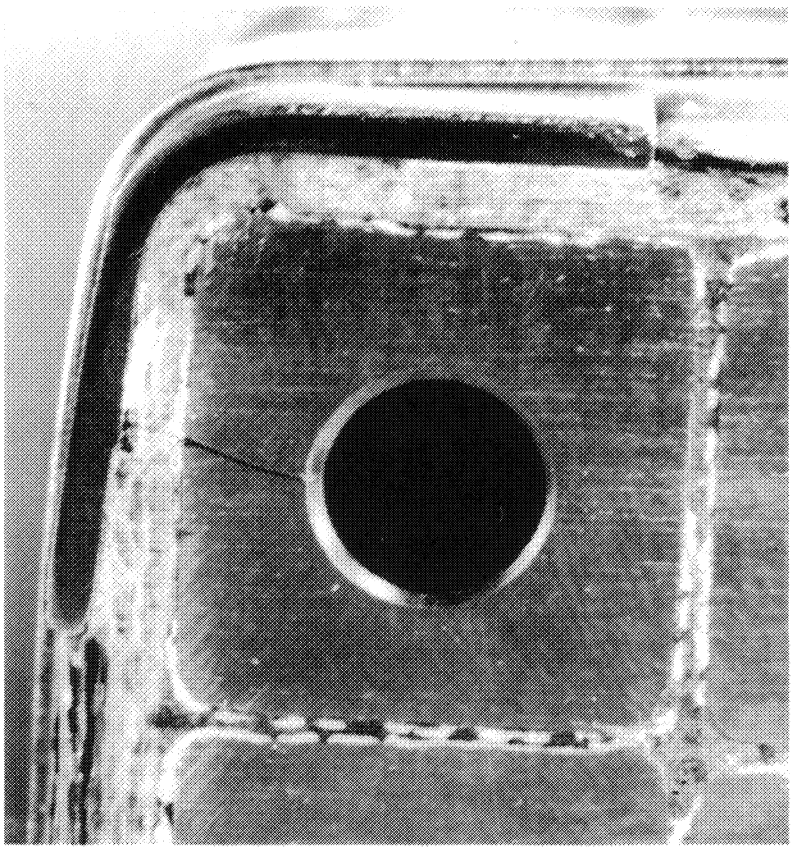

Fig. 22 Detail of bending magnet coil showing corner conductor and ground insulation

Between coil and core the potential drop may amount to several hundred volts. The high-quality ground insulation therefore consists of overlapping layers of 0.8 to 1.0 mm thick bonded mica board. The corner insulation is made of silicone-epoxy-impregnated mica-glass tape which is also non-tracking. This is illustrated in Figs. 21 and 22, and also in Fig. 38.

The shear strength of the insulation is improved by hot-wrapping the straight parts of the coil with a stainless-steel band, which provides compressive forces in the radial direction.

The coil is protected against humidity, and against the corrosive environment which contains nitric acid and ozone, by an airtight casing made of a stainless-steel sheet.

The insulation is dried by heating under vacuum, using a vacuum-drying installation, after which the coil is filled with dry nitrogen to atmospheric pressure.

The asbestos cement gives dimensional stability to the coil; the mica board provides a high-quality insulation; the stainless-steel banding maintains the mechanical integrity of the coil, even when the concrete tends to fissure; the airtight casing ensures good electrical insulation under difficult operating conditions.

Coils for bending magnets are square in cross-section. The hot-wrapped banding applies forces to four metal sections instead of three. Therefore, for the same compressive stress the band should be somewhat thicker. Apart from this, there is no difference with respect to quadrupole coils.

3.7.3 Coil-banding computations

The function of the coil banding is to hold the ground insulation sheets firmly in position and to improve the cohesion between concrete and conductors by applying a radial pressure.

A calculation of the distribution of the compressive stresses generated by the banding has been made with the finite element program SAP applied to the quadrupole coil cross-section.

The two-dimensional, 1 mm thick model used is shown in Fig. 23. It is made up of 42 square copper conductors separated by a 1 mm thick layer of asbestos cement. The assumption is made that the materials behave elastically without cracking. The forces applied to the corner pieces correspond to a stainless-steel band of 0.6 mm thickness, stressed to 20 daN/mm^{2}by thermal shrinkage. They are scaled down for the 1 mm thick model. The coil ends are assumed to be free and the longitudinal stresses are equal to zero (plane stress analysis).

The results of the analysis are given on the figure, where the deformation is drawn with a magnification of 100 for clarity, and the stresses in each insulating layer are given in daN/mm^2.

As expected, the radial compression achieved is maximum on the corners and gradually diminishes towards the centre of the cross-section. However, the desired effect of putting the assembly under compression to give it dimensional stability is achieved.

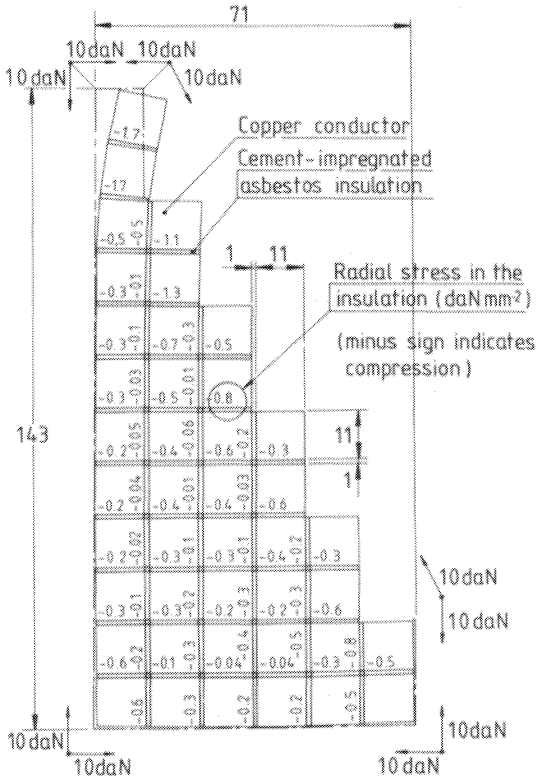

Fig. 23 QNL-B coil model used for finite-element calculation

3.7.4 Special tooling

Some special tooling is required which is not normally found in the tooling-park of an electrotechnical industry. For instance, in the past, in the specific case of a large order, CERN has produced all the special equipment, manufactured a number of prototype coils for testing the procedure, and then handed all this to the successful tenderer[57].

Apart from a concrete mixer, the following special tooling would be required:

- A magnetic sieve and vibrator to eliminate all ferrous particles from the cement and aggregate.
- A pressure mould proper to a specific model of coil.
- A cement impregnation bath, which is in general adapted to a specific coil shape in order to reduce the amount of excess grout to be thrown away after moulding.
- A hot-wrapping tool for stainless-steel banding, which may be used for different types of coils, depending on the coil section and the distance between the legs.
- A vacuum-drying installation which could be used for a range of coils up to a maximum length or width.
- A coil measuring bench, if the geometry of the coil warrants this, specific for each shape of coil.

3.7.5 Coil assembly technique

The coil assembly consists of the following production sequence:

Sandblasting. The impregnated coil resembles a reinforced concrete beam. Good adhesion between copper and cement is important. The sandblasting is therefore somewhat coarser than normal and the surface roughness is specified as N10 grit.

Conductor brazing, coil insulation, and coil forming. These steps are quite well known. The important point is that the coil should be perfectly wound because any waviness will damage the mechanically weak asbestos tape. The coil heads especially should be carefully wound and excessive winding pressures avoided. For an 8 × 8 mm conductor, a 20 mm wide tape was used with a 24 mm pitch to prevent overlapping in the bends.

The tape has to be heat-treated for reasons explained in Section 2.3.6.

After winding has been completed and the terminals have been brazed, the coil is given its correct shape by a system of straps and wooden blocks, followed by the customary hydraulic, dimensional, and electrical checks.

Impregnation. The distance between conductors is temporarily increased by inserting Teflon spacers, 3 to 5 mm thick, as shown in Figs. 24 and 25. The cooling ducts have to be sealed. Thereafter the coil is soaked in clear tap water and allowed to drip dry before impregnation.

Prior to mixing with water, the dry cement powder has to be swept magnetically in order to remove all electrically conducting ferrous matter. This turns out to be mainly inoffensive Fe_2O_3. The vibrator-mounted sieve used for this purpose (see Fig. 26) consists of a container which holds the cement, an adjustable slit for regulating the flow, and a number of permanent magnets, potted in epoxy so as to present a smooth surface which can easily be swept clean. The cement then passes through a coarser sieve (which recuperates any screws worked loose from the vibrator) into a plastic bag which is then sealed and weighed.

The cement powder is then mixed with water in the ratio of 2:1 parts by weight, using a very clean cement mixer. The grout is poured into the impregnation tank after filtering.

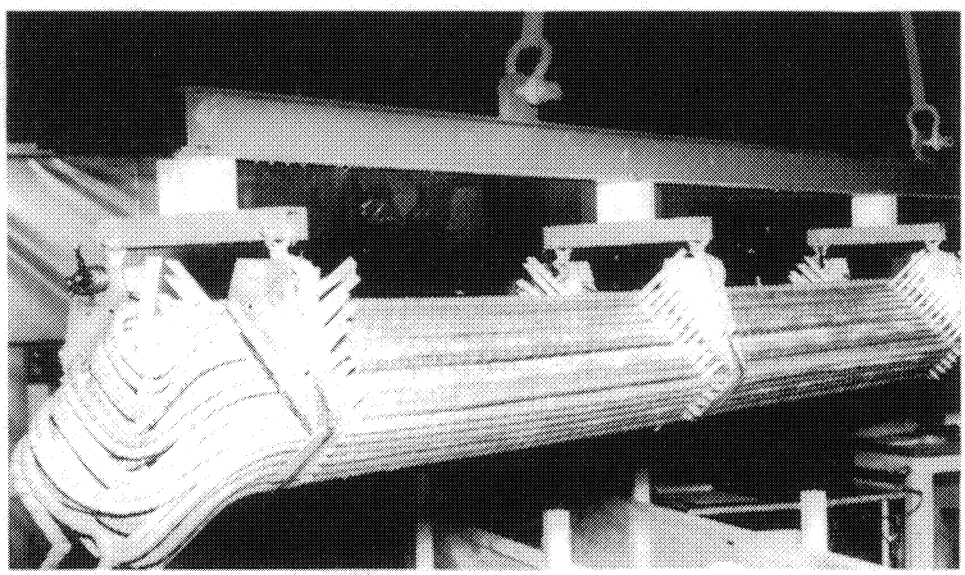

Fig. 24 Quadrupole coil expanded with teflon spacers

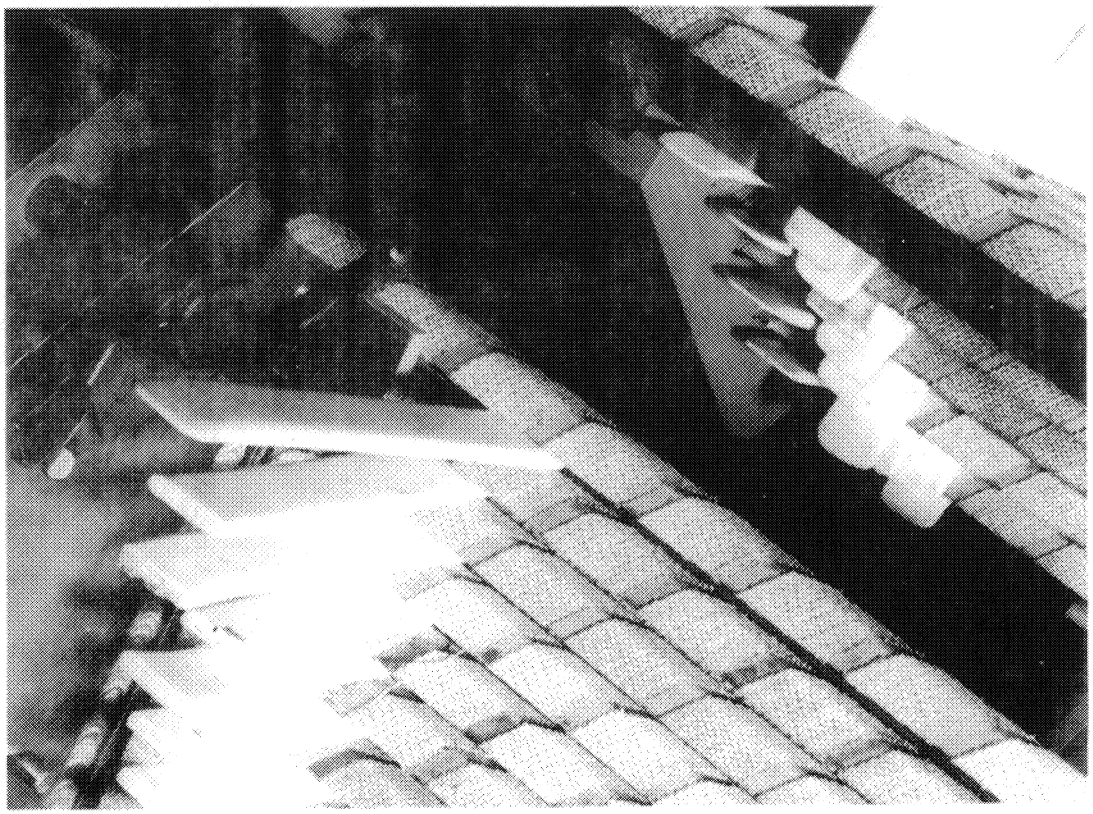

Fig. 25 Close-up of asbestos wrapping and teflon spacers

Fig. 26 Magnetic sieve mounted on a vibrator platform

The cement consists of particles of very different densities, and especially the heavy Fe_2O_3 tends to settle in a few minutes. A fluidized suspension is created by injecting compressed air through a system of perforated tubes which are laid on the bottom of the bath. The cement will now stay at least 10 minutes in suspension. However, the heavy component will still form a cone-shaped deposit centred around each orifice. The mixture has to be stirred vigorously by hand every 10 to 15 minutes.

The coil is then lowered into the bath shown in Fig. 27, impregnated during 2 to 5 minutes, lifted out, and placed on cross-bars over the top of the tank.

The impregnation cannot last for too long a time because the cement settles preferentially on horizontal surfaces, forming a trapezoidal pile-up which cannot be compressed. Thus the vertical dimensions of the coil will no longer fit the mould.

Once the coil is lying on the cross-bars, the spacers are pulled out and the expanded coil is closed. The final configuration is obtained by using two rails and a number of stepped wedges pressed against the inside of the coil by means of a plastic band tightened with specially designed ratchets, as shown in Fig. 28.

Moulding. The moulding operation gives the coil the correct shape by compressing the straight parts and potting the coil heads with high-alumina concrete.

The cross-section of a quadrupole mould is shown in Fig. 29. The stepped wedges placed at intervals along the length of the coil prevent displacement of the conductors. The grooves into which these wedges are fitted in the mould are clearly visible in Fig. 30. The side covers and pressure plates are positioned using hydraulic jacks, as depicted in Fig. 31. The end covers complete the mould shown in Figs. 31 and 32.

The coil heads are potted with concrete using Corindon (Al_2O_3) as the aggregate. The ratio of cement, water, and Corindon is 2:1:4 parts by weight. For compacting, a manually operated pneumatic vibrator is pressed against the mould near the coil heads.

The triangular spaces on the inside of the coil are filled with the more fluid cement grout through ducts provided in the mould for this purpose.

Demoulding takes place after 24 hours. The coil is lifted out of the mould by means of the release screws shown schematically in Fig. 29, an operation which is facilitated by treating the mould with a demoulding agent before use.

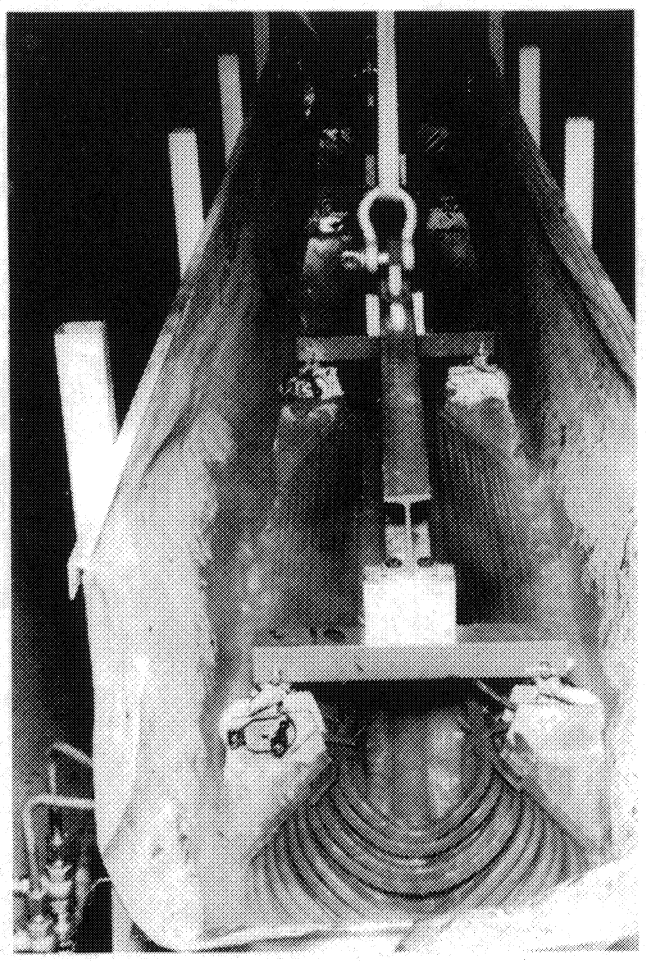

Fig. 27 Impregnation of a coil in a fluidized high-alumina cement bath

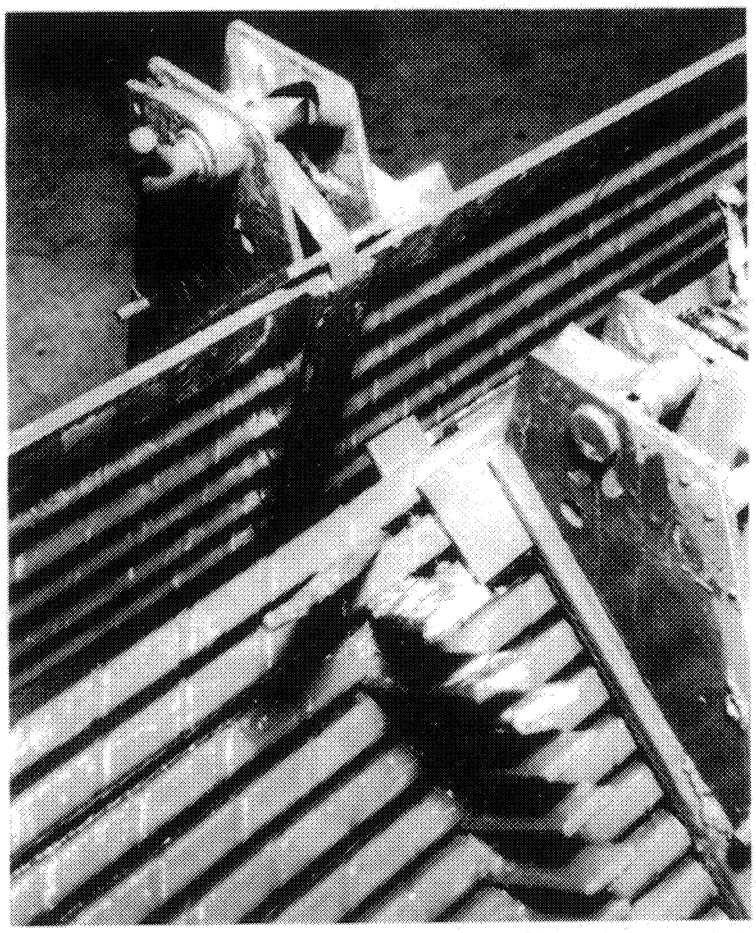

Fig. 28 Close-up of the impregnated coil showing the stepped wedges on the inside and rachets on the outside of the coil

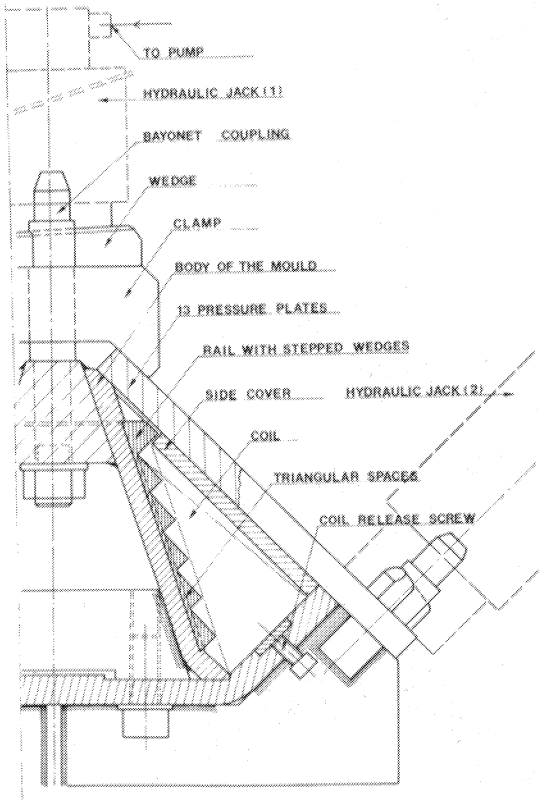

Fig. 29 Cross-section of a quadrupole coil mould

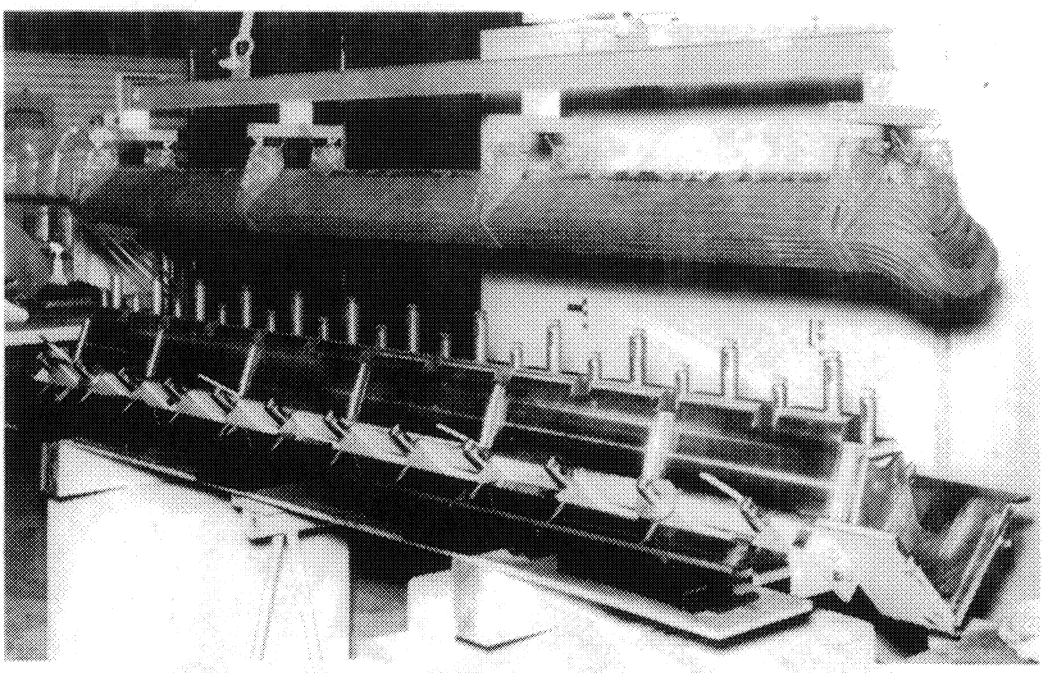

Fig. 30 Lowering the impregnated coil into the compression mould

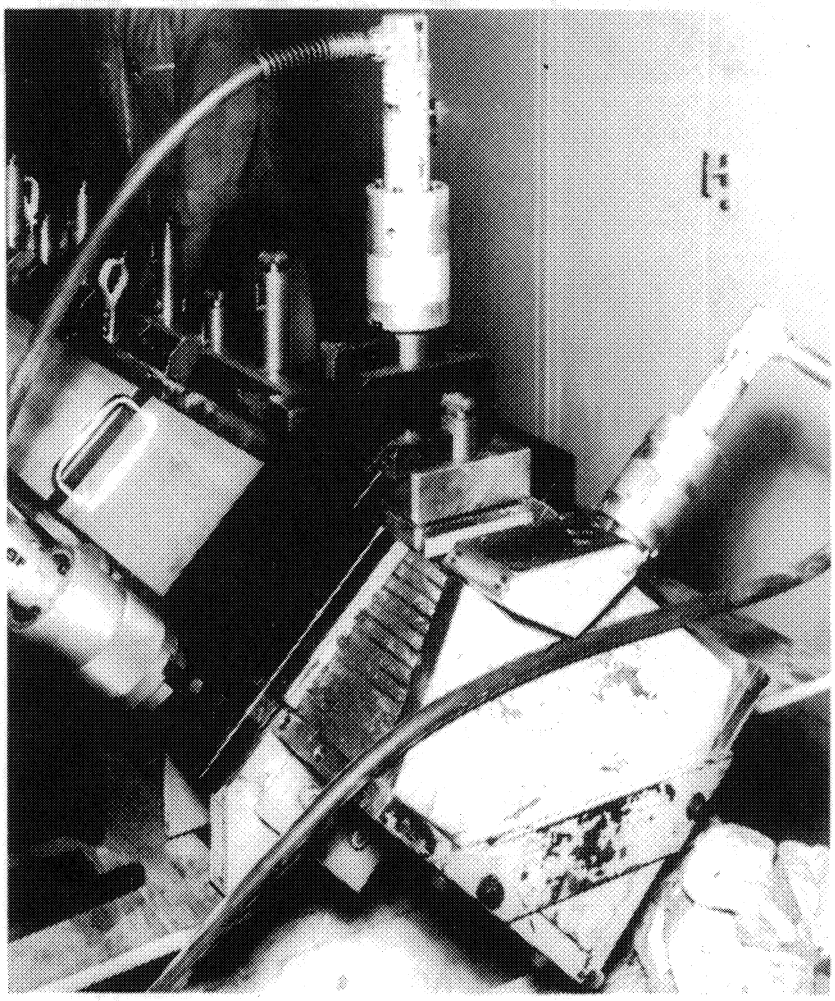

Fig. 31 Compressing a set of pressure plates

Fig. 32 A closed quadrupole mould

The electrical resistance of the cementatious insulation is high compared with that of the coil. The coil resistance may therefore be monitored during the moulding process, to check for possible short circuits between windings. In that case the mould must be designed in such a way that nowhere does the bare conductor touch the electrically conducting walls.

Impregnated coils, after curing and demoulding, are shown in Figs. 33 and 34. The potted parts of the coil heads are clearly visible. Small imperfections are touched-up with a ceramic cement.

Preliminary drying. The resistivity of the asbestos cement after demoulding is of the order of $10^6\ \Omega \cdot mm$. This is too low for induction or capacitor discharge inter-turn testing. The cement should therefore be dried to $10^{10}\ \Omega \cdot mm$, which is the equilibrium value for contact with the ambiant humid atmosphere.

The installation shown in Figs. 35 and 36 dries up to four coils simultaneously. The procedure used is basically that of freeze-drying. A freezer unit cools a vapour trap (the condenser) to $-60\,°C$. The coil is then slowly heated in vacuum, releasing first the water absorbed in the porosities. After this initial quick release of the absorbed water at

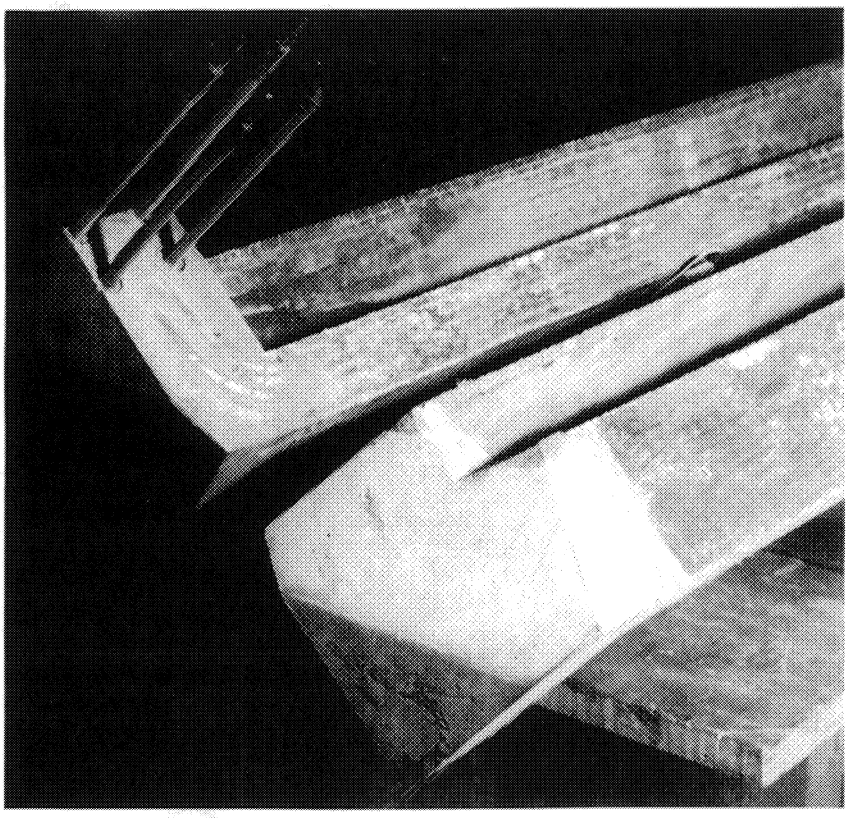

Fig. 33 Cured quadrupole coils

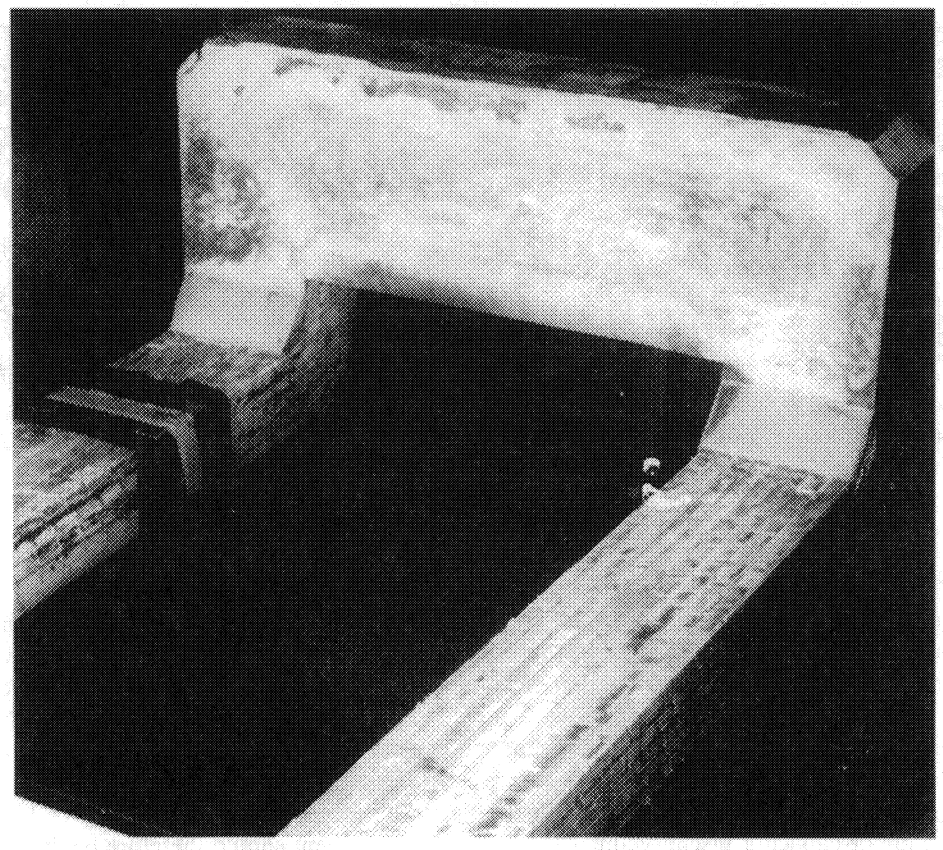

Fig. 34 Cured bending magnet coil

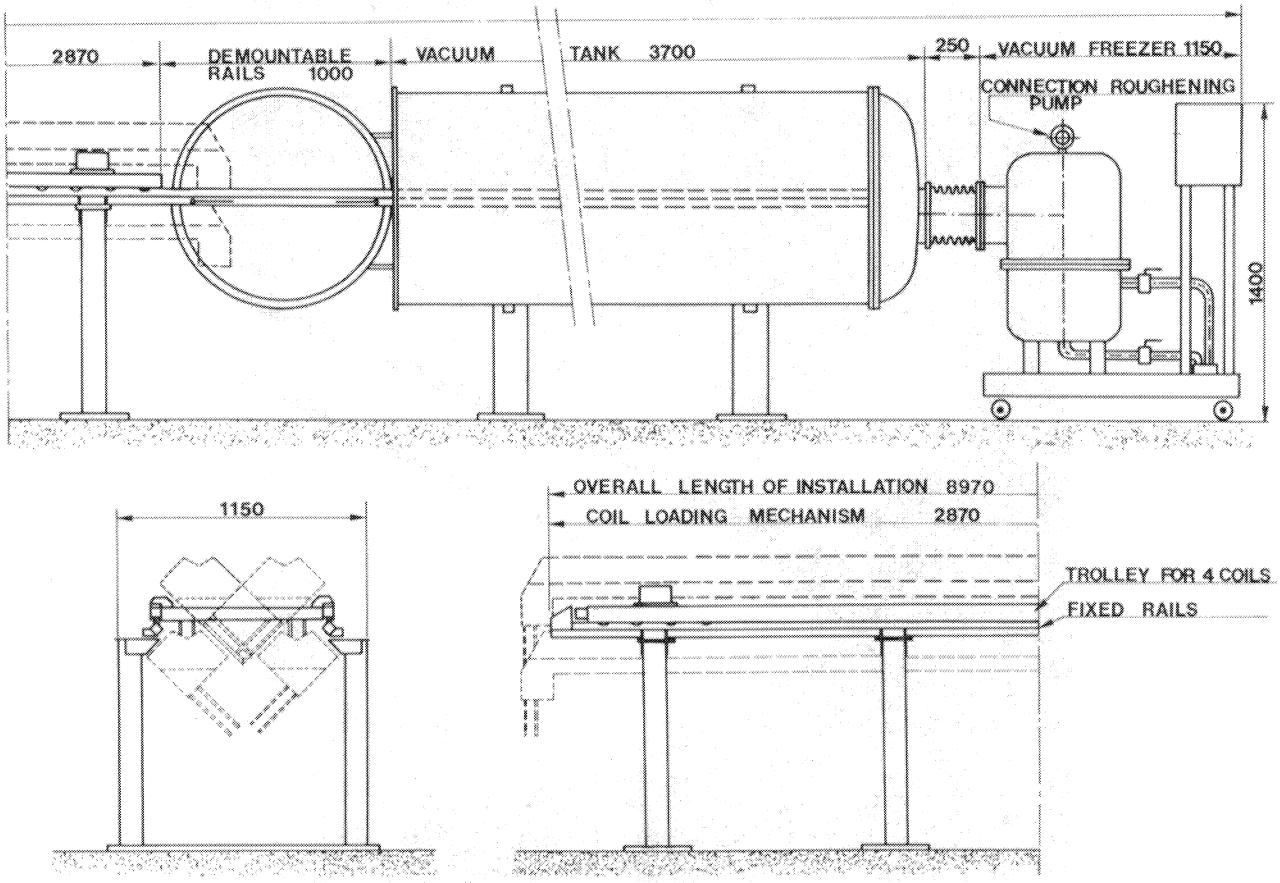

Fig. 35 The vacuum drying installation

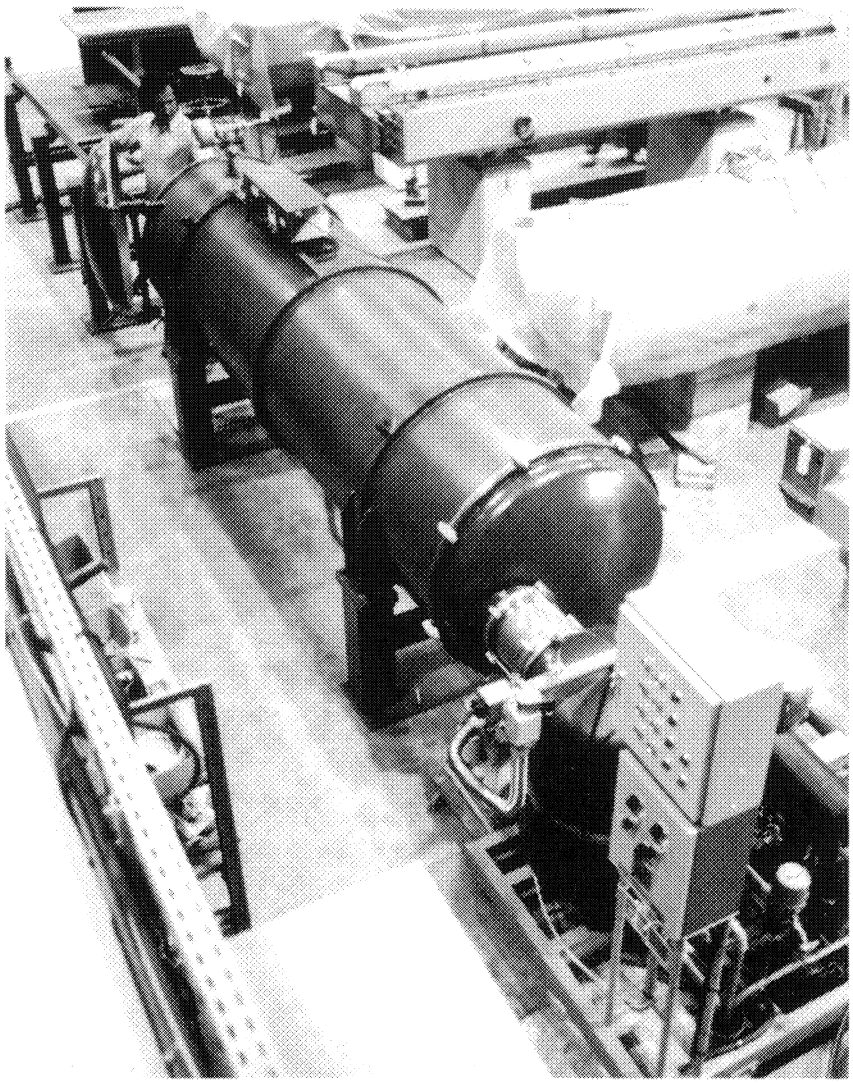

Fig. 36 Bird's-eye view of the vacuum-drying installation

room temperature, mainly during the first day, there follows a gradual loss of the absorbed water as the temperature is raised another 10 °C. Then at higher temperatures the crystal water is released, and is trapped on the condenser walls. Typical drying curves are shown in Fig. 37.

The quantity of water released per coil is 2–3 l, and the total volume of cement, asbestos, and concrete is 17–18 l; the porosity is therefore very high.

The drying installation is composed of three units: the coil-loading trolley; the vacuum tank proper; and the cooling unit with condenser and roughening pump. The coils are mounted on a trolley (see also Fig. 48), which is guided by rails. The trolley is wheeled inside the tank, which contains all the necessary connections for thermocouples, current lead-throughs for Joule heating, etc. After removing the two lengths of rails, the lid of the tank is then closed.

Intermediate electrical testing. The preliminary drying is followed immediately by some electrical tests, because it is important to eliminate weak coils at this early stage. It is also relatively easy to detect the exact position of a short circuit and to repair the cementatious insulation locally.

The CERN quadrupole has two parallel windings, which are in contact over their entire length. The cross-section is shown in Fig. 20. The conductors belonging to a particular winding form alternate layers, and are shown differently cross-hatched in the figure. This configuration is ideal for measuring the resistivity and dielectric strength of the inter-turn insulation.

Experience gained during the construction of a large number of coils is summed up in Table 8. The breakdown voltage between conductors corresponds well to the value found for two electrodes spaced 0.8 mm apart, in air. The induction test with the two windings in series creates a potential drop of 210 V between alternate layers. The value of 10 V per turn was imposed by the size of the transformer available. The induction test should not be interpreted in the ordinary sense where a homogeneous dielectric is tested for holes. The cement is, by nature, full of porosities, holes, and other imperfections such as cracks and inhomogeneities due to bad mixing of the constituents.

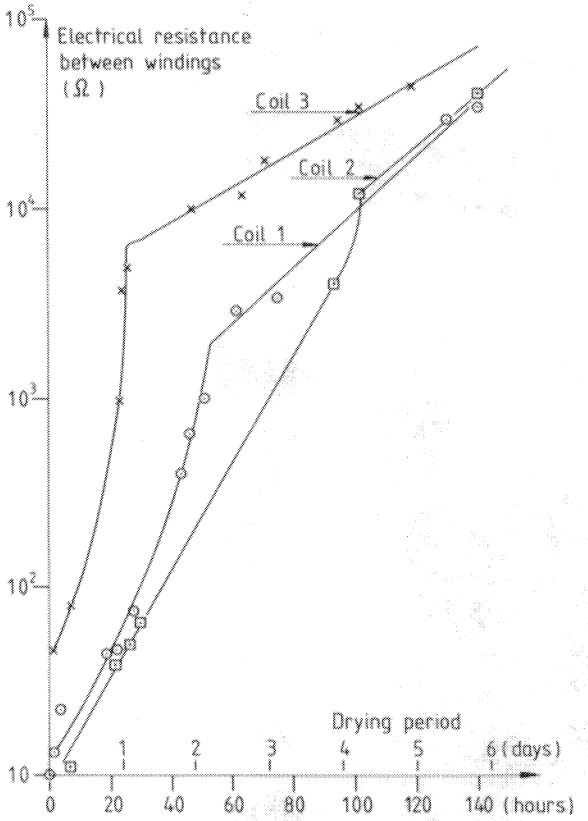

Fig. 37 Preliminary drying of the coils

Table 8

Intermediate electrical test results for quadrupole coils

Number of conductors per coil:	42
Insulated conductor size (mm):	11.5 × 11.5
Total contact area between the two windings (mm^2):	2.84×10^6
Average insulation thickness (mm):	0.86
Resistivity of the concrete (Ω · mm)	
after demoulding:	$1.5–3 \times 10^6$
after preliminary drying:	$3–8 \times 10^{10}$
after final drying:	$3–20 \times 10^{15}$
Resistance between the two windings in the mould (Ω):	1
Resistance of one winding (mΩ):	30
Breakdown voltage between conductors (V d.c.)	650–750

Electrical testing of interturn insulation:

- Measurement of insulation resistance at 500 V d.c.
- Apply tension of 150 V a.c. for 1 minute.
- Repeat insulation resistance measurement; the change should be less than 10%.
- Induction test with two windings in parallel with 10 V per turn, to be followed by induction test with two windings in series, also 10 V per turn.

Mounting of the ground insulation. The ground insulation of the quadrupole coil is shown in Figs. 38 and 39.

Silicone-epoxy-impregnated mica-glass tape is used to insulate the edges, using small amounts of Eastman Kodak contact adhesive. The silicone-epoxy is non-tracking, and radiation will reduce the resin to silica powder. The quantity of tape is small so that the gas release is minimized.

Then follow the layers of overlapping bonded mica-board, 0.8 to 1.0 mm thick, and the stainless-steel corner pieces which distribute the compressive forces exerted by the stainless-steel band. The ground insulation is kept in place by a few turns of mica-glass tape wrapped around the coil.

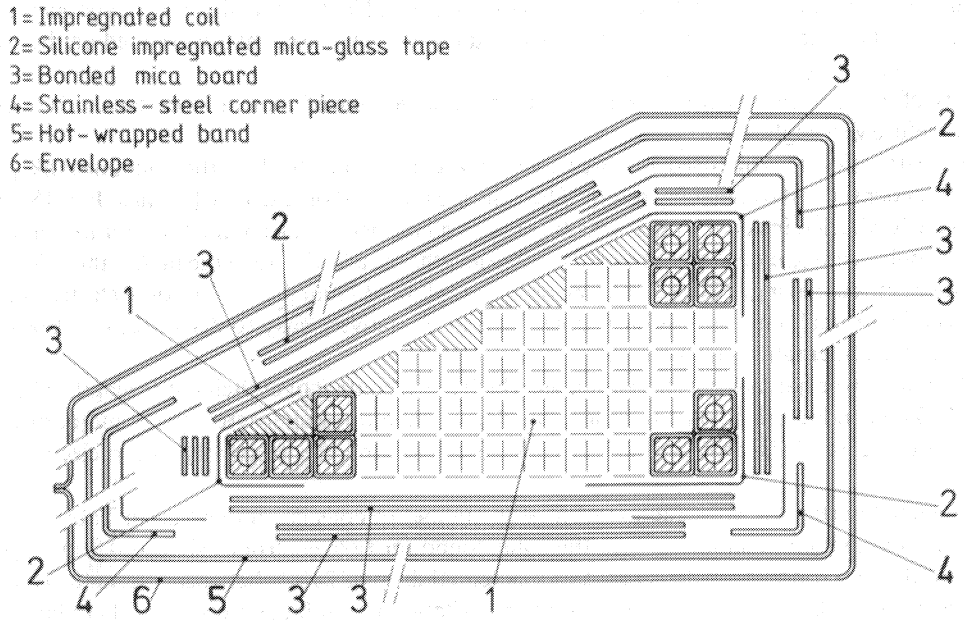

Fig. 38 Cross-section of a quadrupole coil

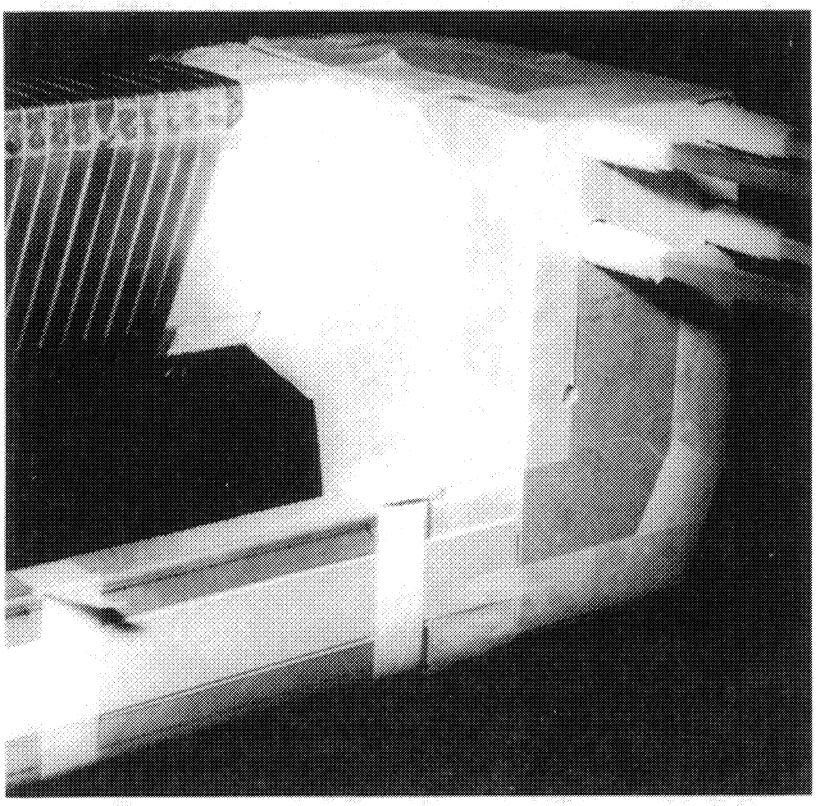

Fig. 39 Coil head with ground insulation mounted and one banded coil-leg

Stainless-steel banding. The band is hot-wrapped around the coil using the Mark I (large ring diameter) and Mark II (small ring diameter) band-wrapping machines shown in Figs. 40 to 42.

A pneumatic compression mechanism presses the ground insulation and the metal sections firmly against the coil before banding.

The tape-winding head consists of two semicircular segments which are separated to remove the coil. A stabilized a.c. power supply is used to heat the tape to roughly 800 °C in order to induce the necessary stresses in the tape by shrinkage. The slack is usually not very much, so that the band is stretched beyond its elastic limit and deforms plastically. The tensile stresses in the band are therefore of the order of 20 daN/mm^2. The stabilization of the power supply should be able to cope with 100% load variations to keep the current and therefore the temperature constant. This is very important if the winding has to be halted for a short period of time, or for a start-up after a long interval. The electrical circuit includes slip rings on the winding head, and spring-loaded carbon brushes to transfer the electrical current to the tape.

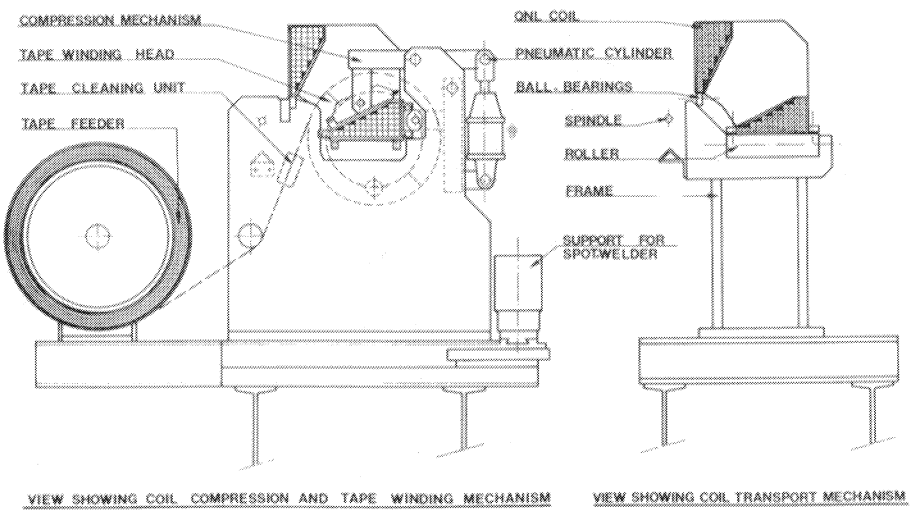

Fig. 40 Diagram of the Mark II band-wrapping machine shown with a quadrupole coil

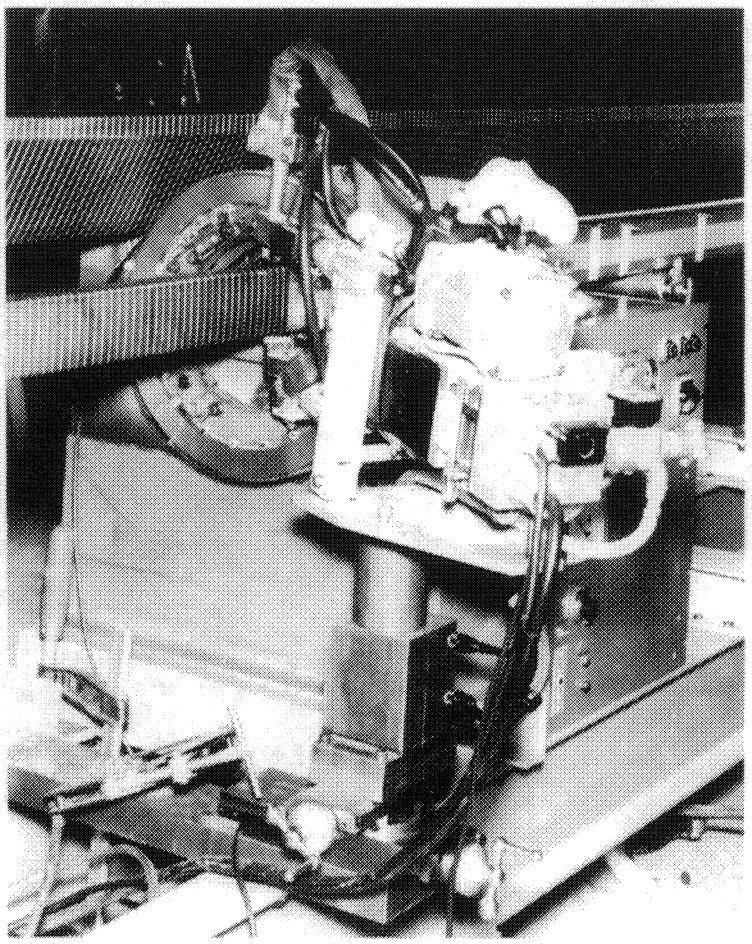

Fig. 41 The Mark II band-wrapping machine with a quadrupole coil

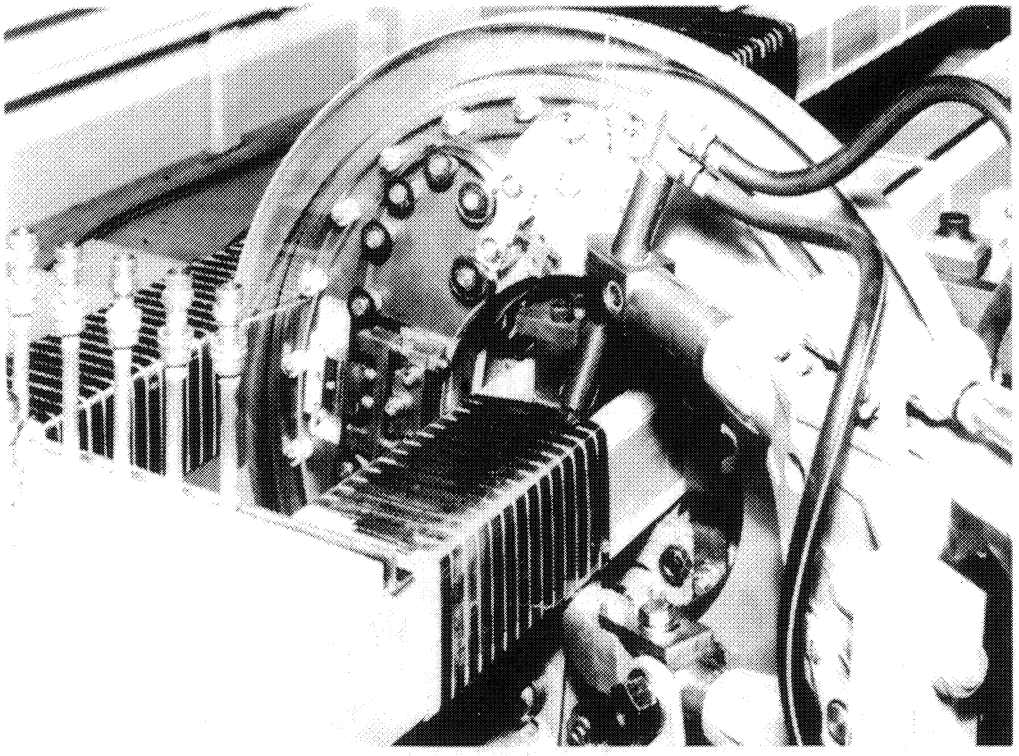

Fig. 42 Close-up of Mark I band-wrapping machine with 2 m flat coil

The quantity of tape that is necessary for one straight leg is stored on the outer rim of the winding head. The tape has to be cleaned chemically prior to loading so as to remove grease which would otherwise impair the electrical contact.

A spot welder completes the wrapping machine. By attaching the tape to the metal corner section after each complete turn, slipping of the band is avoided and a more effective compression of the ground insulation is obtained. Simultaneously, a better protection is obtained against breaking of the band or interruption of the winding process. Finally, the total torque exerted on the coil, compared with the case where only the two end-points of the tape would be spot welded, is reduced by at least 50%. This could be an advantage where long coils are concerned, as these might otherwise become warped.

The quadrupole coils, for example, have been wound with 0.6 × 10 mm stainless-steel band and a pitch of 12 mm.

Assembly of the casing. The airtight casing is made of stainless-steel sheeting. The construction is shown in Figs. 43 to 45. The assembly proceeds as follows.

First the coil-head covers are positioned and very tightly clamped. Subsequent shrinkage of the welds will compress the 2 to 5 mm thick covers even more, and an effect similar to that of hot-wrapping will be obtained. The section on coil mechanics (Section 2.2) explains why the coil-head construction is very important for the behaviour of the coil, especially under pulsed operation.

Then follow the straight sections, 0.8 mm thick. The joint between the thin shell and the thick coil-head casing requires a lot of attention because the weld should be absolutely smooth so as not to compromise fitting in the core. This is done by chamfering the thick plate to the thickness of the shell. The two sheets are then mounted, slightly overlapping, and welded.

The coil geometry is now checked, using the measuring bench shown in Figs. 46 and 47.

Finally, the lead-throughs are positioned and welded. The construction is designed in such a way (see Figs. 44 and 45) that a damaged lead-through may be easily replaced. This is done by grinding away the two circular weldings, one at the base and the other near the conductor.

Leak testing may be done with a helium or freon detector. The leak rate should be less than 1 $Pa \cdot l \cdot s^{-1}$ of air. Because the coil is not completely dry, outgassing is heavy and the highest sensitivity of the leak detection may not be obtained.

Coil geometry check. The easiest way to ensure that each coil will fit is to use as reference an existing core, quadrant, or core-model. The casing of each coil is hand-assembled; the dimensions therefore show small variations. This is not the case with epoxy-moulded coils, which are all produced from the same mould. In addition the coil has a very flexible casing, and it has to be compressed with a considerable force before dimensional checks can be made.

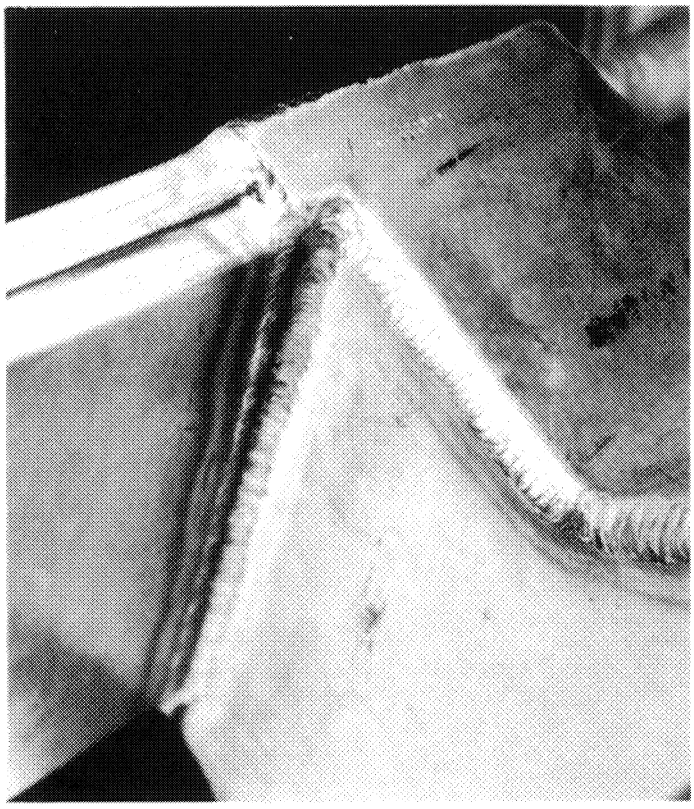

Fig. 43 Welded casing showing transition from 1.0 mm sheeting to 5.0 mm plate, as seen from the inside of the coil

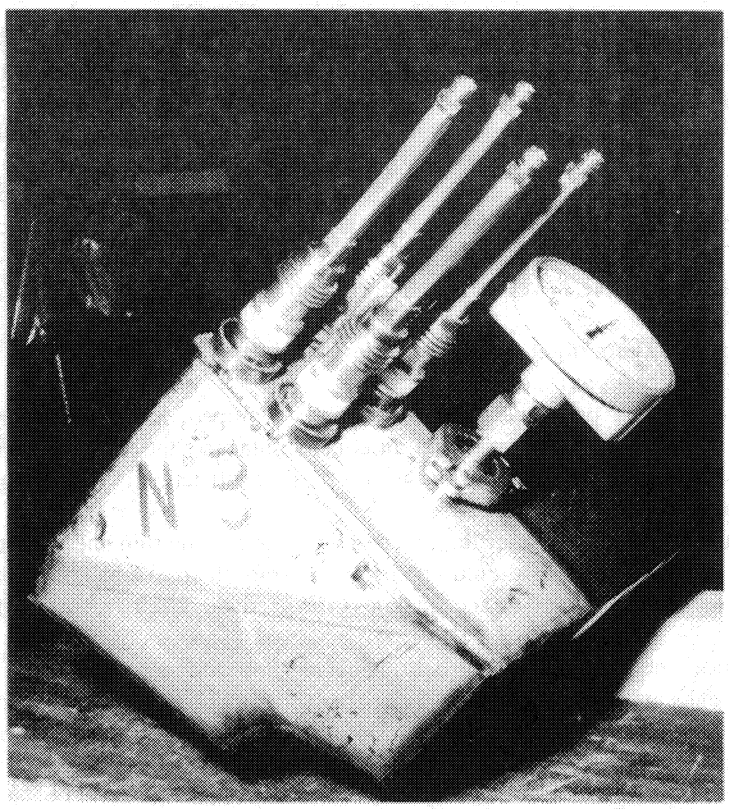

Fig. 44 Construction of the current lead-throughs

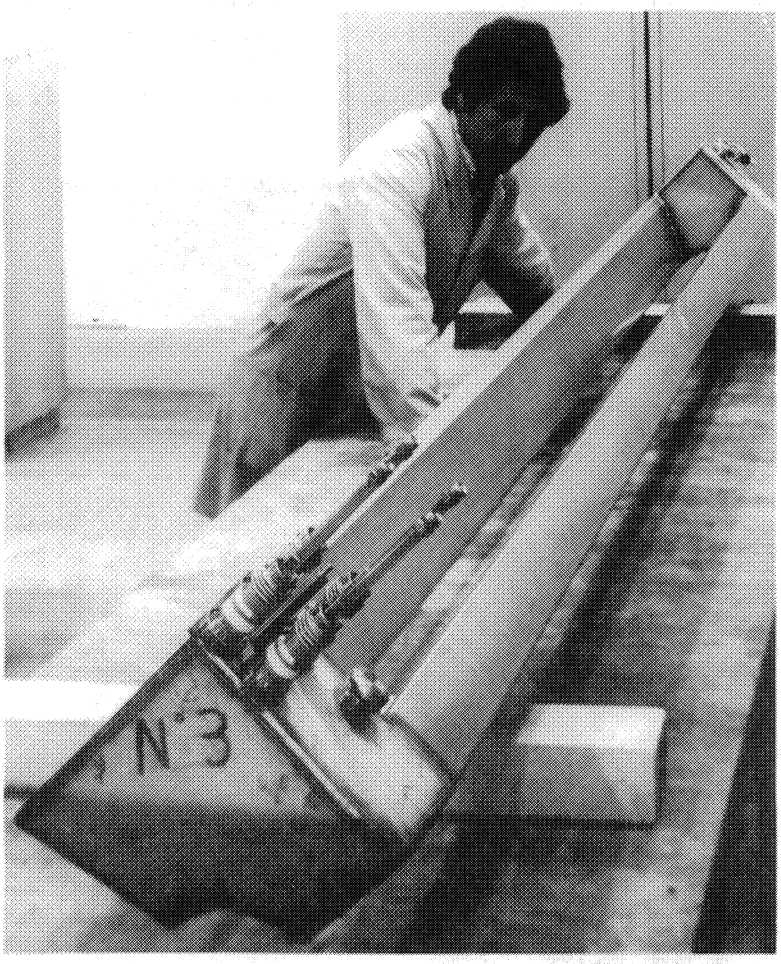

Fig. 45 Completed coil, showing the connection for gas filling at the far end

For these reasons it was decided to construct a dedicated measuring bench based on an existing quadrant, which is shown in Figs. 46 and 47. Its purpose is two-fold. The size of the finished coil is checked, and the thickness and position of the welded-on metal levelling-spacers is determined. By means of the spacers, the straight legs are adjusted to such a level that, with a predetermined compressive force, the coil flanks coincide with the median planes of the quadrant, as demonstrated in Figs. 46 and 48.

The bench consists of the said quadrant, which is mounted on the three supports shown in Fig. 47. The symmetry-axis of the pole is directed vertically upwards, enabling the coil to be lowered by overhead crane and clamped in position.

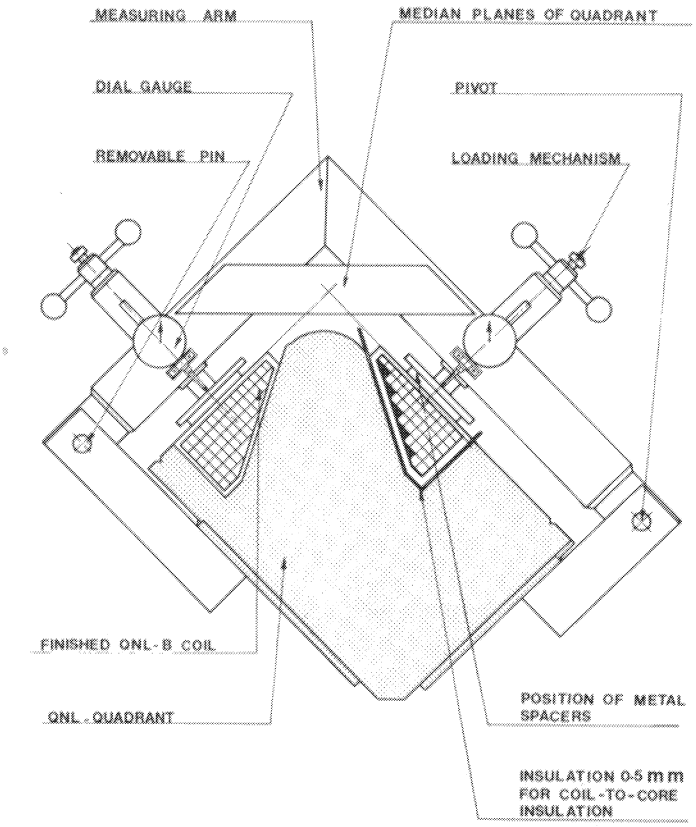

Fig. 46 Cross-section of the coil measuring bench

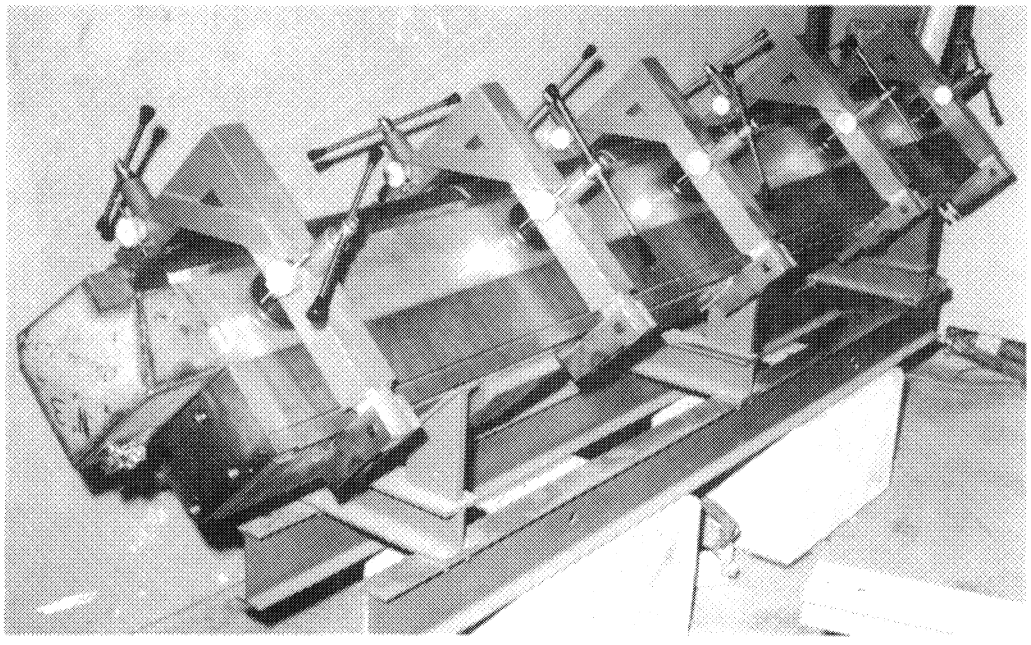

Fig. 47 The quadrupole coil measuring bench

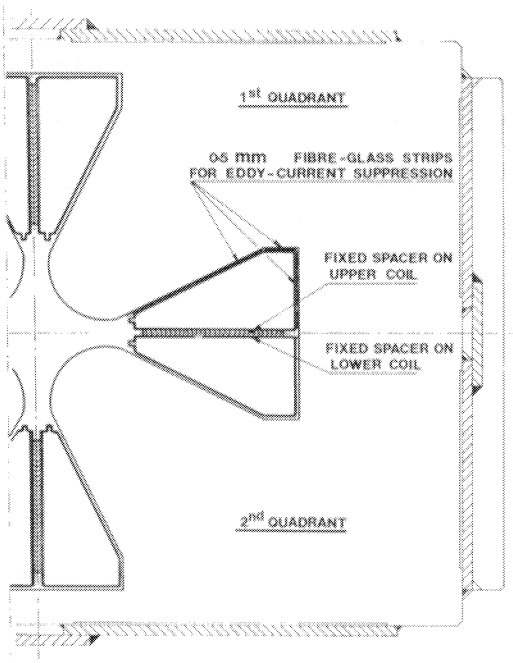

Fig. 48 Position of spacers between the coils

The pressure is exerted by five L-shaped arms, each carrying two loading mechanisms and two dial gauges for measuring the position of the coil flanks. The arms, which are fixed to the sides of the quadrant, pivot about a horizontal axis. They may be swung out of the way by removing a cylindrical blocking-pin. The clamping force per loading mechanism is adjustable between zero and 5000 N.

Final drying. The coil will have a resistance to much higher shearing forces with the banding completed and the coil heads consolidated. The drying temperature may then be raised to 100 °C. The resistivity of the insulation will now increase to between 10^{14} and 10^{15} $\Omega \cdot$ mm. For this purpose, two 32 mm diameter openings have been provided in the coil heads, as shown in Fig. 45, through which the water vapour escapes. Hermetic sealing is obtained by using metal gaskets. A trolley loaded with four coils ready to be dried is shown in Fig. 49.

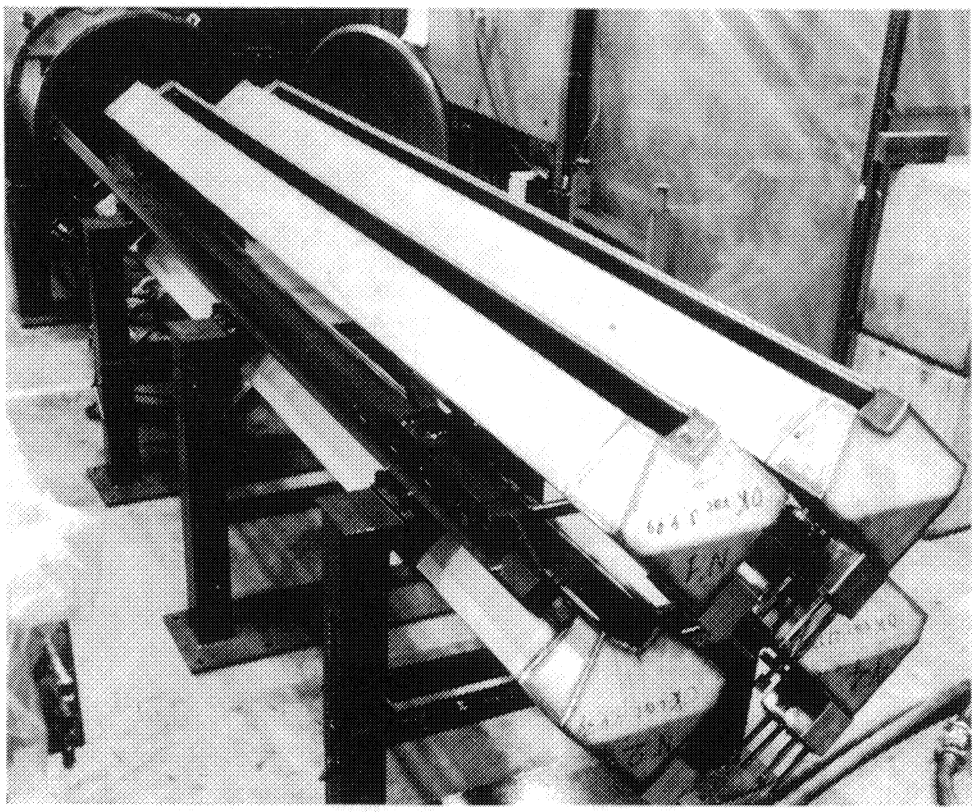

Fig. 49 Final drying, trolley loaded with four quadrupole coils

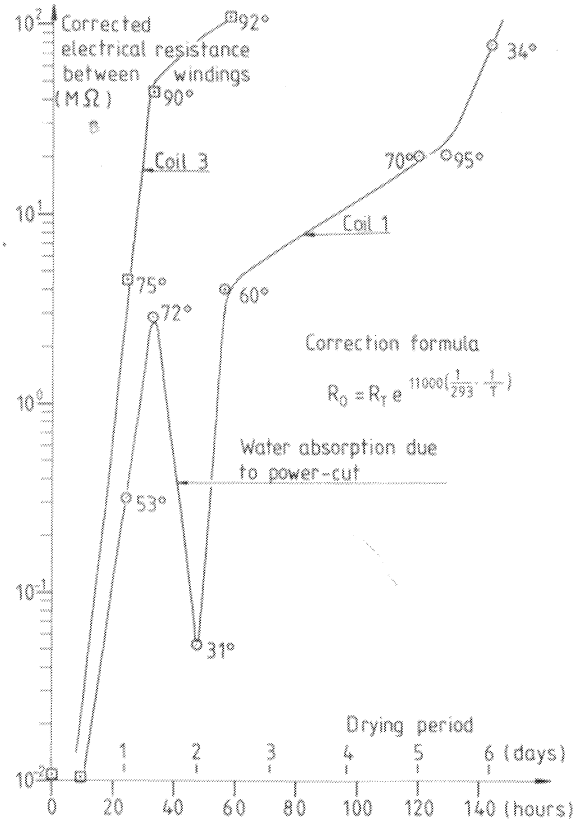

Fig. 50 Final drying curves

Typical final drying curves are shown in Fig. 50. The quantity of water lost during this operation varies between 1.5 and 2.0 l. The initial outgassing is fast because of the temperature increase.

There are several ways of determining the resistivity of the insulation: if the coil is made of several pancakes, the electrical resistance between two windings may be measured; alternatively a humidity gauge, made of two parallel flat or cylindrical electrodes, may be embedded in the coil heads. Another possibility would be to paint a conducting electrode on the outside of the moulded coil and to measure the resistance between the electrode and the coil.

The resistivity is a function of humidity and temperature. To relate the measured resistance R_T to the value at room temperature R_{20}, an expression of the form

$$R_{20} = R_T \exp \alpha \, (1/293 - 1/T)$$

may be used. The parameter α has to be evaluated empirically. Great care must be taken when interpreting values measured on wet coils, because the wet cement functions as an electrolyte, and potential differences of 0.5 V are easily generated.

The vacuum tank is filled with dry nitrogen to atmospheric pressure once the resistivity is satisfactory. The coils then have to be removed and quickly sealed, after which the nitrogen pressure is increased to 0.12 daN/mm^2. The manometer for monitoring the pressure in the coils during storage or transport can be seen in Fig. 44.

It will be necessary to repeat the leak test because heating of the coil to 100 °C might have caused the envelope to rupture. The detection is much more sensitive now, because the coil outgasses much less than before final drying.

Electrical acceptance testing. The electrical tests mentioned in Table 8 are now repeated, excluding the induction test. The latter will be much less effective because of the eddy-current shielding provided by the conducting casing.

In addition, the ground insulation may now be tested. For the quadrupoles, the test is specified as follows:

- The resistance measured between coil and casing, tested with 2500 V d.c., should exceed 1 GΩ.
- Then follows, during one minute, a 2500 V a.c. dielectric test.
- Finally, the d.c. resistance at 2500 V should not have changed by more than 10%.

Actually, the values registered vary between 8 and 12 GΩ.

3.7.6 Assembly of cores and coils

The mechanical and the electrical behaviour of radiation-hardened coils are quite different in some respects from that of epoxy-impregnated ones.

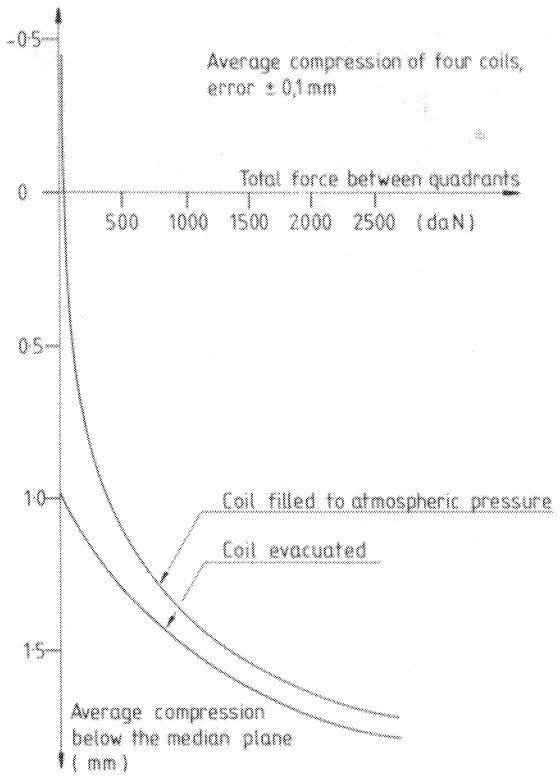

Fig. 51 Compression of the quadrupole coils

The metal casing of the radiation-hardened coil is electrically conducting. If the magnet is pulsed, eddy currents will be generated which could cause undesirable effects, such as field perturbations or heating. Eddy currents may be reduced by insulating the coil from the core, using 0.5 to 1.0 mm thick epoxy/fibre-glass laminates, as illustrated in Fig. 48. The friction between core and coil is thereby also lessened. The forces generated by differential expansion between coil and core are generally much weaker, and the possibility of damaging the thin casing is therefore greatly decreased.

Radiation-hardened coils are not very rigid laterally. The space between the individual layers of bonded mica-board, stainless-steel banding, and casing allows for considerable compression. This natural elasticity is an advantage, so that the use of conventional polyurethane or other elastic organic padding becomes superfluous.

The compression, averaged over four prototype quadrupole coils[58], is shown in Fig. 51. The clamping force between the quadrants, for magnets equipped with epoxy-impregnated coils, is of the order of 2000 daN. With radiation-hardened coils, the same value is obtained using 3.2 mm thick spacers mounted between the two, 20 × 100 mm, levelling spacers, which are permanently attached to the coils. The coil mounting could be facilitated in special cases by evacuating the coils during assembly.

3.7.7 Manifolding

Typical radiation-hardened magnets are shown in Figs. 52 to 54[59,60].

The lead-throughs on the quadrupole coils are protected against mechanical shock by means of metal covers, insulated by ceramic half-cylinders, the two shells being fitted around the conductors.

The cooling circuit has been designed to be corrosion resistant. The manifolding consists of stainless-steel tubing only. The water lead-throughs are made of silicon-powder-filled epoxy resin and embedded stainless-steel end-pieces for screwed connections. With the short insulating distances available, it turned out that electrochemical corrosion in the brazed-on metal end-pieces of ceramic insulators occurred too frequently. Furthermore, many insulators were broken during mounting, because of inherent stresses in the ceramic near the metal end-pieces. The lead-throughs are mounted in one plane on the side of the magnet to facilitate easy replacement.

The standoffs for water tubing and electrical conductors are made of mica-glass blocks and silicone-epoxy impregnated mica paper. The protective wiring which constitutes the interlock system has a fibre-glass sleeving and is mounted in mica-board strips, providing a double electrical insulation.

The magnets are installed without instruments, except for radiation-resistant thermostats mounted in the hot outlet of the coils. Pressure and temperature readings are done remotely.

The magnets are equipped with base-plates; to these are fitted the fast plug-in devices which automatically link power, cooling, and interlock connections. In many cases, also the vacuum connections are operated remotely.

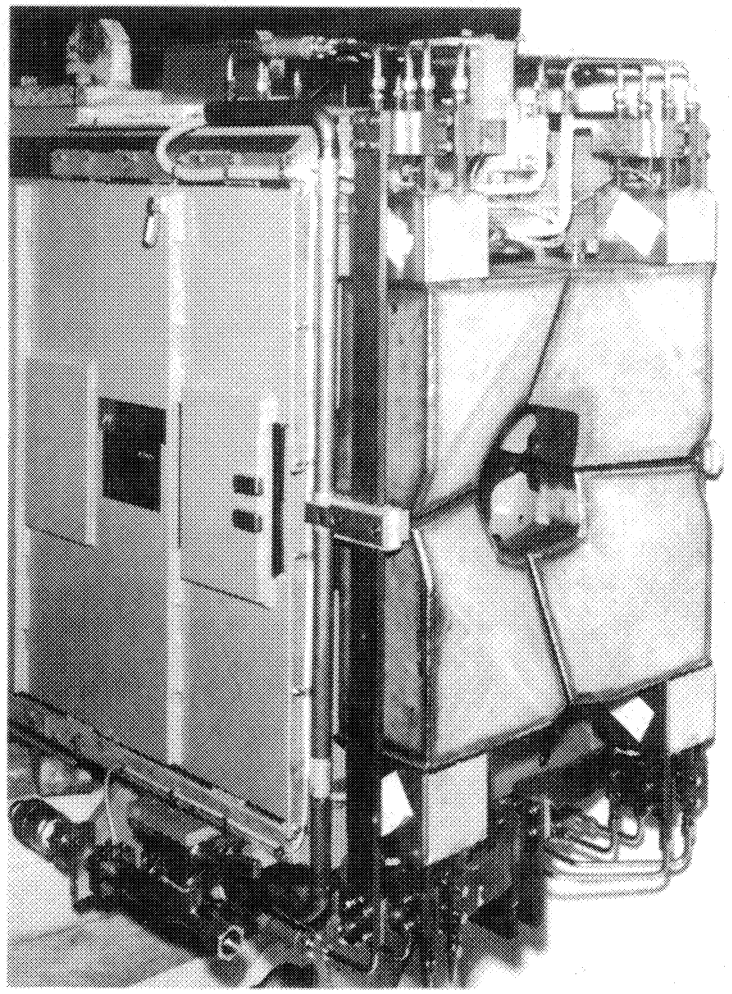

Fig. 52 Radiation-hardened QNL-B quadrupole

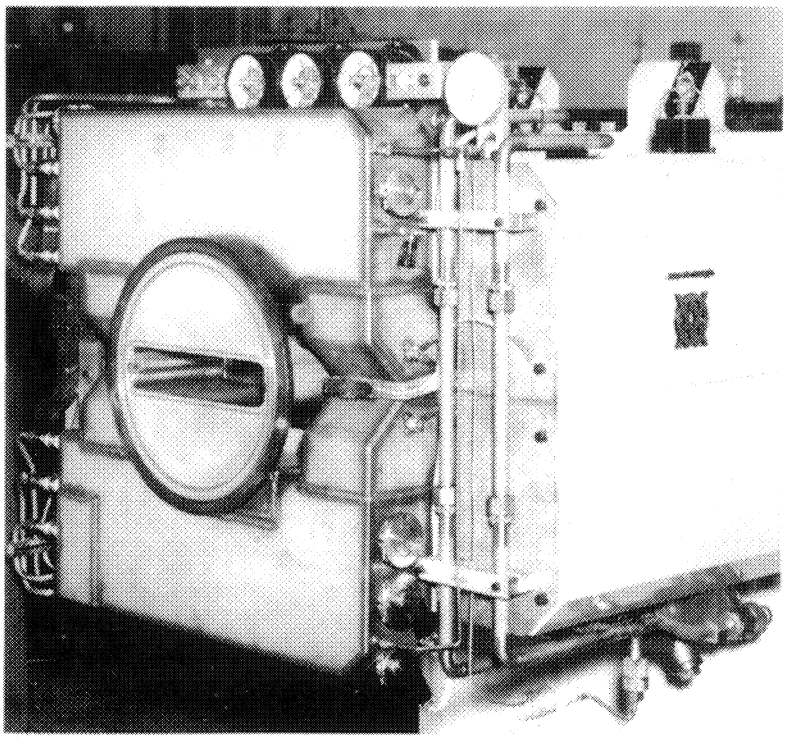

Fig. 53 Radiation-hardened MT magnet

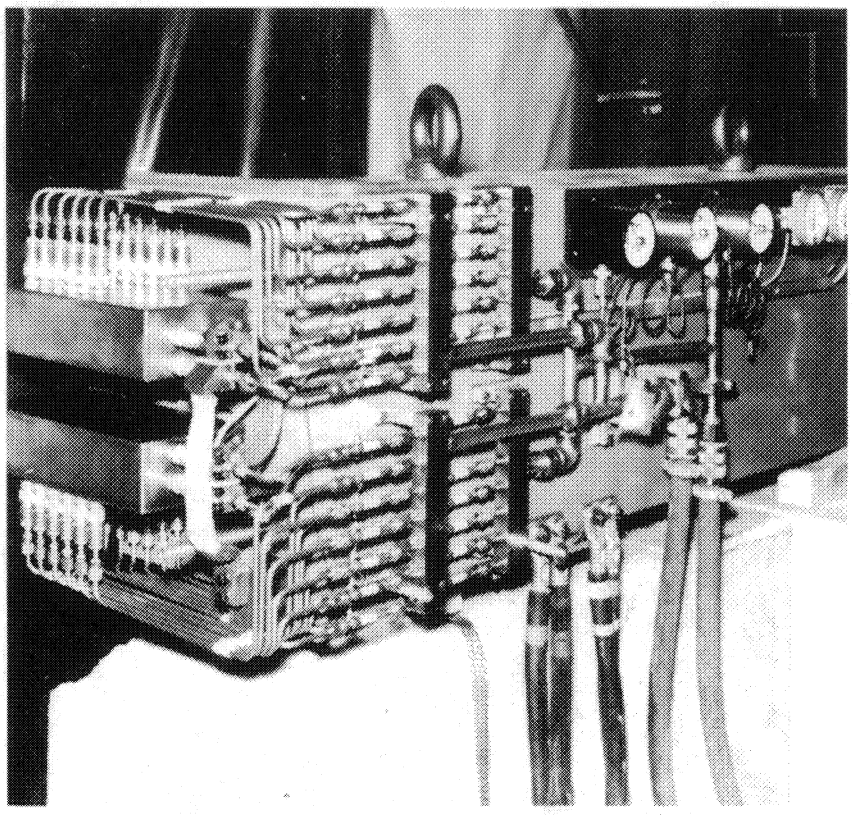

Fig. 54 Rear view of the radiation-hardened MNP 19/C bending magnet

3.7.8 Coil characteristics

The parameters pertaining to flat, saddle-shaped, and quadrupole coils constructed using cementatious impregnation are shown in Table 9.

The filling factor is very close to that of conventional epoxy coils. In effect, in all cases the coils replace conventional types and therefore fit in the same space and carry the same excitation current.

The interturn dielectric strength is much less than is the case with conventional coils, but nevertheless it is largely sufficient for most applications.

The QNL-B coils are slowly pulsed. The thermal time constant is large. After an initial temperature rise, the variation during cycling remains within a few degrees.

Table 9

Some relevant parameters of radiation-resistant magnets constructed at CERN

Parameters	Magnet type			
	MNP 19/C	MTR B24	MTN B40	QNL-B
Gross weight of magnet (tons)	4	24	24	11
Type	C	H	H	Quadrupole
Gap height/bore (mm)	75	36	60	80
Core length (mm)	2000	3600	3600	3200
Coil type	Flat	Saddle	Saddle	–
Cross-section one leg (mm)	91.5 × 81.5	146 × 92	147 × 96	154 × 81
Coil weight (kg)	2 × 250	2 × 800	2 × 800	4 × 330
Conductor size (mm)	9 × 9	20.5 × 18	16 × 16	10.8 × 10.8
Cooling duct diameter (mm)	6	8.5	7	6.15
Number of turns/coil	56	24	40	42
Temperature rise (°C)	25	20	27	22
Spacer material	Al_2O_3	Al_2O_3	Impregnated asbestos tape	Impregnated asbestos tape
Operation	d.c.	d.c.	d.c.	Slowly pulsed

3.7.9 Slowly pulsed operation

The first project, executed in 1974, was an L-shaped, 1200 mm long model of half of a flat coil consisting of 20 conductors, 12.5 × 12.5 mm each. The conductor insulation was made of 1 mm thick alumina spacers and high-alumina cement. Conductor movement and stresses were recorded by suitably placed dial and strain gauges. The model was then cycled thermally 50,000 times. The temperature difference between adjacent conductors was 8 to 12 °C. No variation of the coil parameters, such as the rigidity, could be detected, the initial stiffness being equal to that of a single solid copper conductor with the same outside dimensions as the model.

The prototype quadrupole magnet has also undergone 50,000 thermal cycles with no deterioration of the insulating properties.

3.7.10 Manufacturing costs

Finally, from the point of view of economy, these coils are not cheap. The investment in tooling is considerable: a hot band-wrapping installation and a drying tank with condenser, which could be replaced by a liquid nitrogen trap. An individual mould would be needed for each type of coil.

The construction of the coil requires more expensive materials, such as a stainless-steel casing with ceramic conductor lead-throughs. During construction the amount of intermediate testing is greater than is normally the case. Excluding tooling, these coils turn out to be three times more expensive than conventional coils, but are at least 100 times more resistant to radiation. There is therefore a gain in the long run.

The CERN method, however, offers a possibility for cases where no other solution, requiring a high filling factor, exists. A typical example is that of a radiation-hardened quadrupole with a high field gradient.

REFERENCES AND FOOTNOTES

1) M.H. Van de Voorde and C. Restat, Selection guide to organic materials for nuclear engineering, CERN 72-7 (1972).
2) M.H. Van de Voorde (editor), low-temperature effects in materials and components for superconducting magnets for high-energy physics applications, CERN 77-03 (1977).
3) R.L. Keizer, Stresses and strains in a system of two straight bars joined by a thin elastic medium, CERN/Lab. II/EA/75-3 (1975).
4) D.C. Philips, The effects of radiation on electrical insulators in fusion reactors, Harwell report AERE-R 8923 (1978).
5) M.H. Van de Voorde, Effects of radiation on materials and components, CERN 70-5 (1970).
6) H. Schönbacher and A. Stolarz-Iżycka, Compilation of radiation damage test data, Part I: CERN 79-04 (1979), Part II: CERN 79-08 (1979), Part III: Accelerating engineering materials and components (in preparation).
7) W.R. Cuming, Ceramic encapsulants, Electronic Design, 25 May 1960.
8) C.H. Vondracek, Inorganic potting compounds for high temperatures, Mater. in Design Engin., Dec. 1964, p. 100.
9) F.M. Clark, Insulating materials for design and engineering practice (John Wiley and Sons, Inc., New York 1962).
10) R.A. Wallaert et al., Effects of radiations on ceramic materials (Chapman and Hall, Ltd., London, 1964).
11) T.S. Elleman and C.W. Townley, Materials as affected by radiation, Modern Materials **4**, 101 (1964).
12) F.J.P. Clarke, Irradiation damage in single crystals of MgO, Phil. Mag. **2**, 607 (1957).
13) D.H. Bowen, The effect of nuclear radiation on the mechanical and chemical properties of ceramics, *in* Chemical and mechanical behaviour of inorganic materials (Wiley Interscience, New York, 1968), p. 585.
14) J.F. Kircher and R.E. Bowman (eds.), Effects of radiation on materials and components (Rheinhold Publishing Co., New York, 1964).
15) A.M. Gage, An irradiation test of some magnet components of the LAMPF linear accelerator, Los Alamos report LA-5566-ms (May 1974).
16) L. de Lorenzo, Thermocouple design and test program for the reactor project, Oak Ridge report ORNL 2686 (1958).
17) N.N. Ault and W.M. Wheildon, Modern flame-sprayed ceramic coatings, Modern Materials **2**, 63 (1960).
18) B.R. Emrich and S.P. Brown, Ten new ways to fabricate ceramic parts, Mater. in Design Engin., May 1968, p. 72.
19) B. Chapman (editor), Science and technology of surface coatings (Academic Press, London, 1974).
20) Publications by Union Carbide Corporation, Coatings Service, Rue de Veyrot 15, 1217 Meyrin 2, Geneva, Switzerland.
21) A.M. Neville, Properties of concrete, 2nd Edition (Pitman Publishing Corporation, New York, 1973).
22) V.B. Dubrovskij et al., The effect of neutron irradiation on certain properties of refractory concretes, At. Energ. (USSR) **21**, 108 (1966) [translated by B. Hodge, CERN Trans. 71-36 (1971)].
23) Yu.S. Cherkinskii et al., Effects of ionising radiation on cements, J. Appl. Chem. (USSR) 43, No. 12, 2777 (1970).
24) B.T. Kelly et al. (UKAEA), The effect of radiation on concrete, 2nd Inf. meeting of Prestressed Concrete and Reactor Vessels, Brussels, 1969 (EUR 4531 extr., 1969), p. 238.
25) M.F. Ellench et al., 4th Int. Conf. on Peaceful Uses of Atomic Energy, Geneva, 1971 (United Nations and IAEA, A/CONF. 49/A 6I3, New York, 1972).
26) G. Yamaguchi et al., Induced radioactivity in concrete blocks of various compositions irradiated in the CERN neutrino facility, report HS-RP/058 CERN (1981).
27) F.M. Clark, Insulating materials for design and engineering practice (John Wiley and Sons, Inc., New York, 1962).
28) S. Wernich and R. Pinner, Surface treatment and finishing of aluminium and its alloys, 4th edition (Robert Draper, Ltd., Teddington, 1972).
29) A. Oechslin, Hartanodisieren von Aluminiumlegierungen, Schweizer Aluminium Rundschau No. 8, 1969.
30) D.R. Gabe, Principles of metal surface treatment and protection (Pergamon Press, Oxford, 1972).
31) K. Halbach, Strong rare earth cobalt quadrupoles, IEEE Trans. Nucl. Sci. **NS-26**, 3882 (1979).
32) R.F. Holsinger and K. Halbach, A new generation of samarium-cobalt quadrupole magnets for particle beam focussing applications, presented at the 4th Int. Workshop on Rare Earth Cobalt Permanent Magnets and Their Application, Hakone Park (Japan), 1979.
33) B.P. Murin et al., Concerning the possibility of using quadrupoles with permanent magnets in linear high-energy proton accelerators, Inst. Exp. Tech. **19 (2)**, 327 (1976).
34) R.F. Holsinger, The drift tube and beam line quadrupole permanent magnets for the NEN proton linac, Proc. 10th Linear Accelerator Conference, Montauk (NY), 1979 [BNL 51134, Upton (NY), 1980], p. 373.
35) N.V. Lazarev and V.S. Skachkov, Tipless permanent magnet quadrupole lens, Proc. 10th Linear Accelerator Conference, Montauk (NY), 1979 [BNL 51134, Upton (NY), 1980], p. 380.
36) Los Alamos Scientific Laboratory Specification, SP-2551-MP6-05 (1971).
37) A. Harvey and R.D. Turner, IEEE Trans. Nucl. Sci. **NS-18**, 892 (1971).

38) A. Harvey, Radiation-hardened magnets using mineral-insulated conductors, Proc. IV Int. Conf. on Magnet Technology, Brookhaven, 1972 [Conf. 720908, USAEC, Washington (DC), 1973], p. 456-468, also Los Alamos report LA-5306-MS (1973).
39) A. Harvey and S.A. Walker, Mineral-insulated magnets for high-radiation environments, IEEE Trans. Nucl. Sci. **NS-16**, 611 (1969).
40) J.C. Rauch et E. Violi, Bobines avec isolation inorganique et leur utilisation dans des électro-aimants de recherche, Rev. Brown Boveri 11-74 (also in English as CH-IM 311050 E).
41) A. Harvey, Experience with the LAMPF mineral-insulated magnets, Proc. Int. Conf. on Magnet Technology, Bratislava, 1977 (ALFA, Bratislava, 1978), p. 551.
42) L. Evans et al., The steel septum magnets for beam splitting at the CERN SPS, CERN report ABT/77-13 (1977).
43) D. George, Magnets with mineral insulated coils at SIN, Proc. Int. Conf. on Magnet Technology, Rome, 1975 (Lab. Naz. CNEN, Frascati, 1975), p. 719.
44) Publication 182 from Pyrotenax of Canada, Ltd., Trenton, Ontario, Canada.
45) L.R. Glasgow and R.J. Burleigh, Trim coil construction for the Berkeley 88 inch Cyclotron, Nucl. Instrum. Methods 18-19, 567 (1962).
46) A. Harvey, Proc. Linear Accelerator Conf., Batavia (Ill.), 1970 [NAL, Batavia (Ill.), 1971], p. 709.
47) R.L. Keizer, Prototype ES septum magnet for the PSB-CPS transfer system, CERN/SI/Int. MAE/71-3 (1971).
48) R.L. Keizer, Prototype 12-turn septum magnet (TSV) for the PSB-CPS transfer line, CERN/SI/Int. MAE/71-4 (1971).
49) E. Roskowski, Experience with aluminium magnet coils, IEEE Trans. Nucl. Sci. **NS-16**, 777 (1969).
50) M.M. Holland and J. Shill, Radiation resistant magnet coils from hard anodized aluminium conductor, IEEE Trans. Nucl. Sci. **NS-20**, 708 (1973).
51) J. Monet, Constitution de la bobine d'éjection du synchrocyclotron, CERN 472-MSC/PR-SB (1969).
52) H.F. Vogel and J.J. Rosenthal, Cement-potted coils for muon channel magnets, Los Alamos report LASL-AEC OFFICIAL, published after April 1972.
53) D.R. Willis and D. Wilson, The design and construction of a concrete-insulated quadrupole magnet, Proc. Int. Conf. on Magnet Technology, Hamburg, 1970 (DESY, Hamburg, 1972), p. 677.
54) A.T. Gresham, R. Sheldon and G.B. Stapleton, Hydrating cements for radiation resistant magnet constructions, Proc. Int. Conf. on Magnet Technology, Hamburg, 1970 (DESY, Hamburg, 1972), p. 1244.
55) A.T. Gresham, R. Sheldom and G.B. Stapleton, Magnets for radiation-resistant accelerators, Part. Accel. **4** (1), 43 (1972).
56) R.L. Keizer and M. Mottier, Mineral insulated magnets, CERN/SPS/EMA 77-3 (1977).
57) Technical specification radiation resistant coils for QNL-B quadrupoles, SPS/EMA/Spec. 78-22 (1978).
58) R.L. Keizer and M. Mottier, Note on the assembly of QNL-B quadrupoles, SPS/EMA/Note 79-13 (1979).
59) R.L. Keizer and M. Mottier, The MTN and MTR bending magnets, SPS/EA/78-15 (1978).
60) R.L. Keizer and M. Mottier, Technical note on the MNP19/C bending magnet, SPS/EA/Note 76-2 (1976).